Death and rebirth of neural activity in sparse inhibitory networks

To cite this article: David Angulo-Garcia *et al* 2017 *New J. Phys.* **19** 053011

View the article online for updates and enhancements.

New Journal of Physics

The open access journal at the forefront of physics

Deutsche Physikalische Gesellschaft ⬥ DPG

IOP Institute of Physics

Published in partnership with: Deutsche Physikalische Gesellschaft and the Institute of Physics
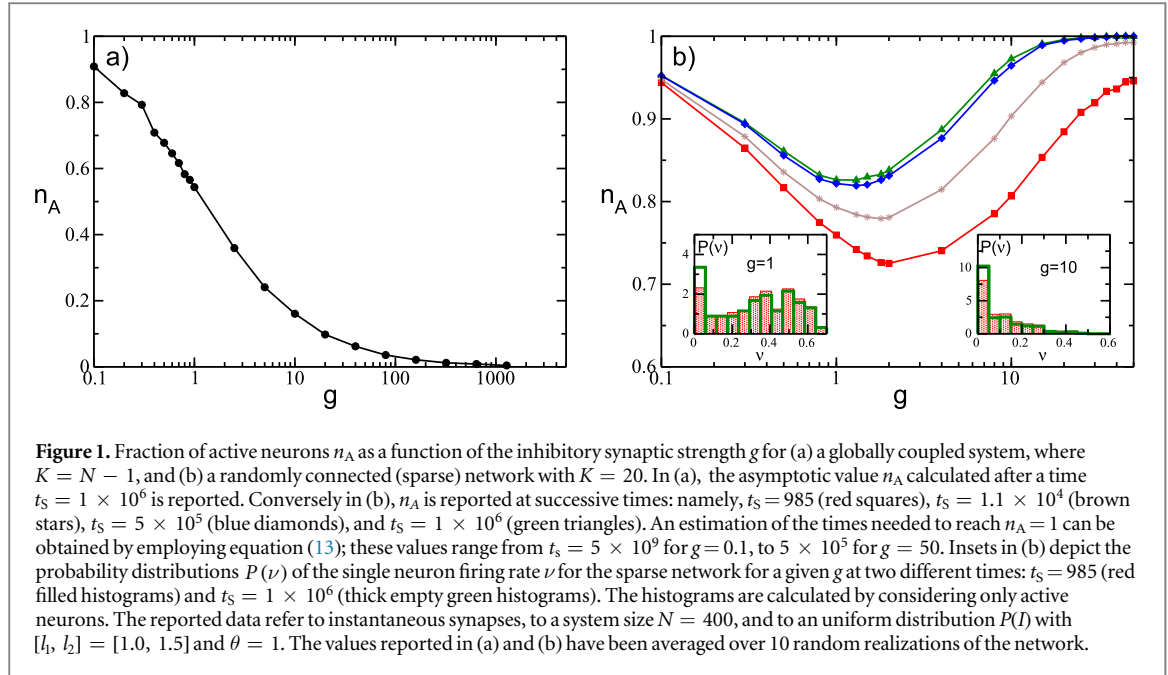
Death and rebirth of neural activity in sparse inhibitory networks

David Angulo-Garcia[1,2], Stefano Luccioli[3,4], Simona Olmi[1,3,5] and Alessandro Torcini[1,2,3,6,7,8]

1 Aix Marseille Univ, INSERM, INMED and INS, Inst Neurosci Syst, Marseille, France
2 Aix Marseille Univ, Université de Toulon, CNRS, CPT, UMR 7332, F-13288 Marseille, France
3 CNR—Consiglio Nazionale delle Ricerche—Istituto dei Sistemi Complessi, I-50019 Sesto Fiorentino, Italy
4 INFN—Istituto Nazionale di Fisica Nucleare—Sezione di Firenze, I-50019 Sesto Fiorentino, Italy
5 Weierstrass Institute, Mohrenstraße 39, D-10117 Berlin, Germany
6 Laboratoire de Physique Théorique et Modélisation, Université de Cergy-Pontoise, CNRS, UMR 8089, F-95302 Cergy-Pontoise Cedex, France
7 Max-Planck-Institut für Physik komplexer Systeme, Nöthnitzer Straße 38, D-01187 Dresden, Germany
8 Author to whom any correspondence should be addressed.

E-mail: david.angulo-garcia@univ-amu.fr, stefano.luccioli@fi.isc.cnr.it, simona.olmi@isc.cnr.it and alessandro.torcini@univ-amu.fr

Abstract

Inhibition is a key aspect of neural dynamics playing a fundamental role for the emergence of neural rhythms and the implementation of various information coding strategies. Inhibitory populations are present in several brain structures, and the comprehension of their dynamics is strategical for the understanding of neural processing. In this paper, we clarify the mechanisms underlying a general phenomenon present in pulse-coupled heterogeneous inhibitory networks: inhibition can induce not only suppression of neural activity, as expected, but can also promote neural re-activation. In particular, for globally coupled systems, the number of firing neurons monotonically reduces upon increasing the strength of inhibition (neuronal death). However, the random pruning of connections is able to reverse the action of inhibition, i.e. in a random sparse network a sufficiently strong synaptic strength can surprisingly promote, rather than depress, the activity of neurons (neuronal rebirth). Thus, the number of firing neurons reaches a minimum value at some intermediate synaptic strength. We show that this minimum signals a transition from a regime dominated by neurons with a higher firing activity to a phase where all neurons are effectively sub-threshold and their irregular firing is driven by current fluctuations. We explain the origin of the transition by deriving a mean field formulation of the problem able to provide the fraction of active neurons as well as the first two moments of their firing statistics. The introduction of a synaptic time scale does not modify the main aspects of the reported phenomenon. However, for sufficiently slow synapses the transition becomes dramatic, and the system passes from a perfectly regular evolution to irregular bursting dynamics. In this latter regime the model provides predictions consistent with experimental findings for a specific class of neurons, namely the medium spiny neurons in the striatum.

1. Introduction

The presence of inhibition in excitable systems induces a rich dynamical repertoire, which is extremely relevant for biological [13], physical [32], and chemical systems [84]. In particular, inhibitory coupling has been invoked to explain cell navigation [87], morphogenesis in animal coat pattern formation [46], and the rhythmic activity of central pattern generators in many biological systems [27, 45]. In brain circuits, the role of inhibition is fundamental to balance massive recurrent excitation [73] in order to generate physiologically relevant cortical rhythms [12, 72].

Inhibitory networks are important not only for the emergence of rhythms in the brain, but also for the fundamental role they play in information encoding in the olfactory system [39] as well as in controlling and regulating motor and learning activity in the basal ganglia [5, 15, 47]. Furthermore, stimulus-dependent

Figure 1. Fraction of active neurons n_A as a function of the inhibitory synaptic strength g for (a) a globally coupled system, where $K = N - 1$, and (b) a randomly connected (sparse) network with $K = 20$. In (a), the asymptotic value n_A calculated after a time $t_S = 1 \times 10^6$ is reported. Conversely in (b), n_A is reported at successive times: namely, $t_S = 985$ (red squares), $t_S = 1.1 \times 10^4$ (brown stars), $t_S = 5 \times 10^5$ (blue diamonds), and $t_S = 1 \times 10^6$ (green triangles). An estimation of the times needed to reach $n_A = 1$ can be obtained by employing equation (13); these values range from $t_s = 5 \times 10^9$ for $g = 0.1$, to 5×10^5 for $g = 50$. Insets in (b) depict the probability distributions $P(\nu)$ of the single neuron firing rate ν for the sparse network for a given g at two different times: $t_S = 985$ (red filled histograms) and $t_S = 1 \times 10^6$ (thick empty green histograms). The histograms are calculated by considering only active neurons. The reported data refer to instantaneous synapses, to a system size $N = 400$, and to an uniform distribution $P(I)$ with $[I_1, I_2] = [1.0, 1.5]$ and $\theta = 1$. The values reported in (a) and (b) have been averaged over 10 random realizations of the network.

sequential activation of a group of neurons, reported for asymmetrically connected inhibitory cells [33, 52], has been suggested as a possible mechanism to explain sequential memory storage and feature binding [67].

These explain the long-term interest for numerical and theoretical investigations of the dynamics of inhibitory networks. The study of globally coupled homogeneous systems have already revealed interesting dynamical features, ranging from full synchronization to clustering appearance [23, 83, 85], and from the emergence of splay states [90] to oscillator death [6]. The introduction of disorder, e.g. random dilution, noise, or other forms of heterogeneity in these systems leads to more complex dynamics, ranging from fast global oscillations [9] in neural networks and self-sustained activity in excitable systems [37], to irregular dynamics [3, 29–31, 42, 49, 56, 82, 90]. In particular, inhibitory spiking networks, due to *stable chaos* [63], can display extremely long erratic transients even in linearly stable regimes [3, 29, 30, 42, 49, 82, 89, 90].

One of the most studied inhibitory neural populations is represented by medium spiny neurons (MSNs) in the striatum (which is the main input structure of the basal ganglia) [36, 57]. In a series of papers, Ponzi and Wickens have shown that the main features of MSN dynamics can be reproduced by considering a randomly connected inhibitory network of conductance based neurons subject to external stochastic excitatory inputs [64–66]. Our study has been motivated by an interesting phenomenon reported for this model in [66]: namely, upon increasing the synaptic strength the system passes from a regularly firing regime, characterized by a large part of quiescent neurons, to a biologically relevant regime where almost all cells exhibit a bursting activity, characterized by an alternation of periods of silence and of high firing. The same phenomenology has been recently reproduced by employing a much simpler neural model [1], thus suggesting that this behavior is not related to the specific model employed, but is indeed a quite general property of inhibitory networks. However, the origin of the phenomenon and the minimal ingredients required to observe the emergence of this effect remain unclear.

In order to exemplify the problem addressed in this paper, we report in figure 1 the fraction of active neurons n_A (i.e. the ones emitting at least one spike during the simulation time) as a function of the strength of the synaptic inhibition g in an heterogeneous network. For a fully coupled network, n_A has a monotonic decrease with g (figure 1(a)), while for a random sparse network, n_A has a non-monotonic behavior, displaying a minimum at an intermediate strength g_m (figure 1(b)). In fully coupled networks the effect of inhibition is simply to reduce the number of active neurons (*neuronal death*). However, quite counter-intuitively, in the presence of dilution by increasing the synaptic strength the previously silenced neurons can return to firing (*neuronal rebirth*). Our aim is to clarify the physical mechanisms underlying neuronal death and rebirth, which are at the origin of the behavior reported in [1, 66].

In particular, we consider a deterministic network of purely inhibitory pulse-coupled Leaky Integrate-and-Fire (LIF) neurons with an heterogeneous distribution of excitatory DC currents, accounting for the different level of excitability of the neurons. The evolution of this model is studied for fully coupled and for random sparse topology, as well as for synapses with different time courses. For the fully coupled case, it is possible to derive, within a self-consistent mean field approach, the analytic expressions for the fraction of active neurons and for the average firing frequency $\bar{\nu}$ as a function of coupling strength g. In this case, the monotonic decrease of n_A

with *g* can be interpreted as a *Winner Takes All* (WTA) mechanism [16, 21, 88], where only the most excitable neurons survive the inhibition increase. For random sparse networks, neuronal rebirth can be interpreted as a re-activation process induced by erratic fluctuations in synaptic currents. Within this framework it is possible to semi-analytically obtain, for instantaneous synapses, a closed set of equations for n_A as well as for the average firing rate and coefficient of variation as a function of the coupling strength. In particular, the firing statistics of the network can be obtained via a mean field approach by extending the formulation derived in [70] to account for synaptic shot noise with constant amplitude. The introduction of a finite synaptic time scale does not modify the overall scenario provided that this is shorter than the membrane time constant. As soon as the synaptic dynamics become slower, the phenomenology of the transition is modified. At $g < g_m$ we have a *frozen phase* where n_A does not evolve in time on the explored time scales, since the current fluctuations are negligible. Above g_m we have a bursting regime, which can be related to the emergence of correlated fluctuations induced by slow synaptic times, as discussed in the framework of the adiabatic approach in [50, 51].

The remainder of this paper is organized as follows: In section 2 we present the models that will be considered in the paper as well as the methods adopted to characterize their dynamics. In section 3 we consider the globally coupled network where we provide analytic self-consistent expressions accounting for the fraction of active neurons and the average firing rate. Section 4 is devoted to the study of sparsely connected networks with instantaneous synapses, and to the derivation of the set of semi-analytic self-consistent equations providing n_A, the average firing rate, and the coefficient of variation. In section 5 we discuss the effect of synaptic filtering with a particular attention on slow synapses. Finally in section 6, we briefly discuss the obtained results with a focus on the biological relevance of our model.

2. Model and methods

We examine the dynamical properties of a heterogeneous inhibitory sparse network made of *N* LIF neurons. The time evolution of the membrane potential v_i of the *i*-th neuron is ruled by the following first-order ordinary differential equation:

$$\dot{v}_i(t) = I_i - v_i(t) - gE_i(t), \tag{1}$$

where $g > 0$ is the inhibitory synaptic strength, I_i is the neuronal excitability of the *i*-th neuron encompassing both intrinsic neuronal properties and the excitatory stimuli originating from areas outside the considered neural circuit, and $E_i(t)$ represents the synaptic current due to the recurrent interactions within the considered network. The membrane potential v_i of neuron *i* evolves accordingly to equation (1) until it overcomes a constant threshold $\theta = 1$, which leads to the emission of a spike (action potential) transmitted to all connected post-synaptic neurons while v_i is reset to its resting value $v_r = 0$. The model in (1) is expressed in adimensional units, this amounts to assume a membrane time constant $\tau_m = 1$; for the conversion to dimensional variables see appendix A. The heterogeneity is introduced in the model by assigning to each neuron a different value of excitability I_i drawn from a flat distribution $P(I)$, whose support is $I \in [l_1, l_2]$ with $l_1 \geqslant \theta$; therefore, all neurons are supra-threshold.

The synaptic current $E_i(t)$ is given by the linear superposition of all the inhibitory post-synaptic potentials (IPSPs) $\eta(t)$ emitted at previous times $t_n^j < t$ by the pre-synaptic neurons connected to neuron *i*, namely

$$E_i(t) = \frac{1}{K} \sum_{j \neq i} C_{ij} \sum_{n|t_n < t} \eta(t - t_n^j), \tag{2}$$

where *K* is the number of pre-synaptic neurons. C_{ij} represents the elements of the $N \times N$ connectivity matrix associated with an undirected random network, whose entries are 1 if there is a synaptic connection from neuron *j* to neuron *i*, and 0 otherwise. For the sparse network, we randomly select the matrix entries; however, to reduce the sources of variability in the network, we assume that the number of pre-synaptic neurons is fixed, namely $\sum_{j \neq i} C_{ij} = K \ll N$ for each neuron *i*, where autaptic connections are not allowed. We have verified that the results do not change if we randomly choose the links accordingly to an Erdös–Renyi distribution with a probability K/N. For a fully coupled network we have $K = N - 1$.

The shape of the IPSP characterizes the type of filtering performed by the synapses on the received action potentials. We have considered two kinds of synapses: instantaneous ones, where $\eta(t) = \delta(t)$, and synapses where the PSP is an α-pulse, namely

$$\eta(t) = H(t)\alpha^2 t e^{-t\alpha}, \tag{3}$$

with *H* denoting the Heaviside step function. In this latter case the rise and decay time of the pulse are the same, namely $\tau_\alpha = 1/\alpha$, and therefore the pulse duration τ_P can be assumed to be twice the characteristic time τ_α. Model equations (1) and (2) are integrated exactly in terms of the associated *event driven maps* for different

synaptic filtering, which correspond to Poincaré maps performed at the firing times (for details see appendix A) [53, 91].

For instantaneous synapses, we have usually considered system sizes $N = 400$ and $N = 1400$, and in the sparse case in-degrees $20 \leqslant K \leqslant 80$ and $20 \leqslant K \leqslant 600$, respectively, with integration times up to $t_S = 1 \times 10^6$. For synapses with a finite decay time we have limited the analysis to $N = 400$ and $K = 20$, and to maximal integration times $t_S = 1 \times 10^5$. Finite size dependencies on N are negligible with these parameter choices, as we have verified.

In order to characterize the network dynamics, we measure the fraction of active neurons $n_A (t_S)$ at time t_S, i.e. the fraction of neurons emitting at least one spike in the time interval $[0, t_S]$. Therefore a neuron will be considered silent if it has a frequency smaller than $1/t_S$, and with our choices of $t_S = 10^5 - 10^6$, this corresponds to neurons with frequencies smaller than $10^{-3} - 10^{-4}$ Hz by assuming a membrane time constant $\tau_m = 10$ ms as time scale. Estimation of the number of active neurons always begins after a sufficiently long transient time has been discarded, usually corresponding to the time needed to deliver 10^6 spikes in the network.

Furthermore, for each neuron we estimate the time averaged inter-spike interval (ISI) T_{ISI}, the associated firing frequency $\nu = 1/T_{ISI}$, as well as the coefficient of variation CV, which is the ratio of the standard deviation of the ISI distribution divided by T_{ISI}. For a regular spike train $CV = 0$, and for a Poissonian distributed one $CV = 1$, while $CV > 1$ is an indication of bursting activity. The indicators reported in the following to characterize network activity are ensemble averages over all active neurons, which we denote as $\bar{a}$ for a generic observable a.

To analyze the linear stability of the dynamical evolution we measure the maximal Lyapunov exponent λ, which is positive for chaotic evolution, and negative (zero) for stable (marginally stable) dynamics [4]. In particular, by following [2, 55], λ is estimated by linearizing the corresponding event driven map.

3. Fully coupled networks: WTA

In the fully coupled case we observe that the fraction of active neurons n_A saturates, after a short transient, to a value that remains constant in time. In this case, it is possible to derive a self-consistent mean field approach to obtain analytic expressions for the fraction of active neurons n_A and for the average firing frequency $\bar{\nu}$ of neurons in the network. In a fully coupled network each neuron receives the spikes emitted by the other $K = N - 1$ neurons; therefore, each neuron is essentially subject to the same effective input $> \mu$, apart from the finite size corrections $\mathcal{O}(1/N)$.

The effective input current, for a neuron with an excitability I, is given by

$$\mu = I - g\bar{\nu}n_A, \tag{4}$$

where $n_A (N - 1)$ is the number of active pre-synaptic neurons assumed to fire with the same average frequency $\bar{\nu}$.

In a mean field approach, each neuron can be seen as isolated from the network and driven by the effective input current μ. Taking into account the distribution of excitabilities $P(I)$, one obtains the following self-consistent expression for the average firing frequency:

$$\bar{\nu} = \frac{1}{n_A} \int_{\{I_A\}} dI \, P(I) \left[\ln\left(\frac{I - g\bar{\nu}n_A - \nu_r}{I - g\bar{\nu}n_A - \theta} \right) \right]^{-1}, \tag{5}$$

where the integral is restricted only to active neurons, i.e. to $I \in \{I_A\}$ values for which the logarithm is defined, while $n_A = \int_{\{I_A\}} dI \, P(I)$ is the fraction of active neurons. In (5) we have used the fact that for an isolated LIF neuron with constant excitability C, the ISI is simply given by $T_{ISI} = \ln[(C - \nu_r)/(C - \theta)]$ [11].
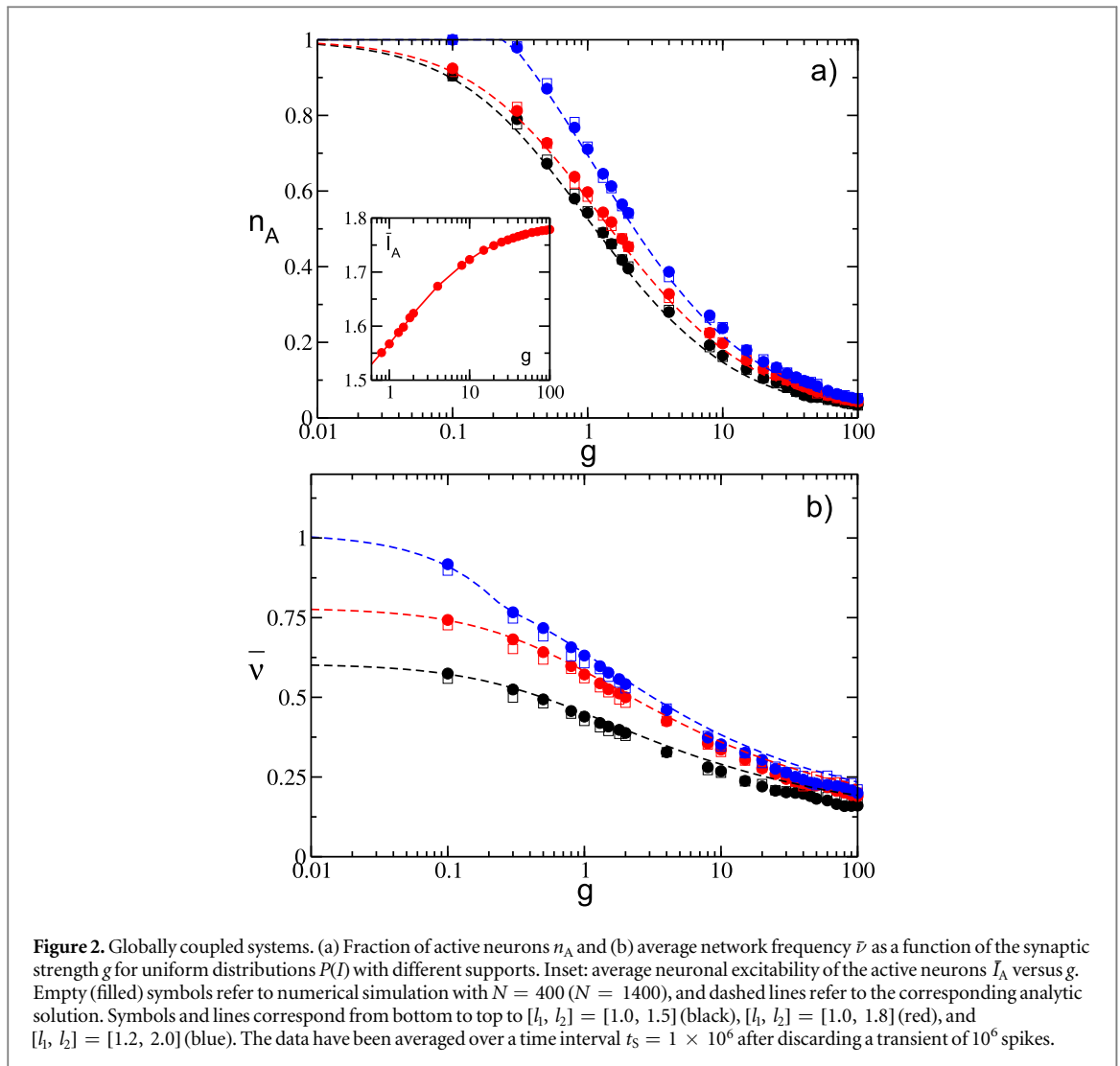
An implicit expression for n_A can be obtained by estimating the neurons with effective input $\mu > \theta$; in particular, the fraction of silent neurons is given by

$$1 - n_A = \int_{l_1}^{l^*} dI \, P(I), \tag{6}$$

where l_1 is the lower limit of the support of the distribution, while $l^* = g\bar{\nu}n_A + \theta$. By solving self-consistently equations (5) and (6), one can obtain the analytic expression for n_A and $\bar{\nu}$ for any distribution $P(I)$.

In particular, for excitabilities distributed uniformly in the interval $[l_1, l_2]$, the expression for the average frequency equation (5) becomes

$$\bar{\nu} = \frac{1}{n_A (l_2 - l_1)} \int_{\{I_A\}} dI \left[\ln\left(\frac{I - g\bar{\nu}n_A - \nu_r}{I - g\bar{\nu}n_A - \theta} \right) \right]^{-1}, \tag{7}$$

Figure 2. Globally coupled systems. (a) Fraction of active neurons n_A and (b) average network frequency $\bar{\nu}$ as a function of the synaptic strength g for uniform distributions $P(I)$ with different supports. Inset: average neuronal excitability of the active neurons $\bar{I}_A$ versus g. Empty (filled) symbols refer to numerical simulation with $N = 400$ ($N = 1400$), and dashed lines refer to the corresponding analytic solution. Symbols and lines correspond from bottom to top to $[l_1, l_2] = [1.0, 1.5]$ (black), $[l_1, l_2] = [1.0, 1.8]$ (red), and $[l_1, l_2] = [1.2, 2.0]$ (blue). The data have been averaged over a time interval $t_S = 1 \times 10^6$ after discarding a transient of 10^6 spikes.

while the fraction of active neurons is given by the following expression

$$n_A = \frac{l_2 - \theta}{l_2 - l_1 + g\bar{\nu}} \qquad (8)$$

with the constraint that n_A cannot be larger than one.

The analytic results for these quantities compare quite well with the numerical findings estimated for different distribution intervals $[l_1, l_2]$, coupling strengths, and system sizes, as shown in figure 2. For definitively large coupling $g > 10$, some discrepancies between the mean field estimations and the simulation results are observable (see figure 2(b)). These differences are probably due to the discreteness of the pulses, which cannot be neglected for very large synaptic strengths.

As a general feature we observe that n_A is steadily decreasing with g, thus indicating that a group of neurons with higher effective inputs (*winners*) silence the other neurons (*losers*) and that the number of winners eventually vanishes for sufficiently large coupling in the limit of large system sizes. Furthermore, the average excitability of active neurons (the winners) $\bar{I}_A$ increases with g, as shown in the inset of figure 2(a), thus revealing that only neurons with higher excitabilities survive the silencing action exerted by the other neurons. At the same time, as an effect of the growing inhibition, the average firing rate of the winners dramatically slows down. Therefore, despite the increase of $\bar{I}_A$, the average effective input $\bar{\mu}$ indeed decreases for increasing inhibition. This represents a clear example of the WTA mechanism obtained via (lateral) inhibition, which has been shown to have biological relevance for neural systems [20, 60, 88].

It is important to understand what is the minimal coupling value g_c for which the firing neurons start to die. In order to estimate g_c it is sufficient to set $n_A = 1$ in equations (7) and (8). In particular, one gets

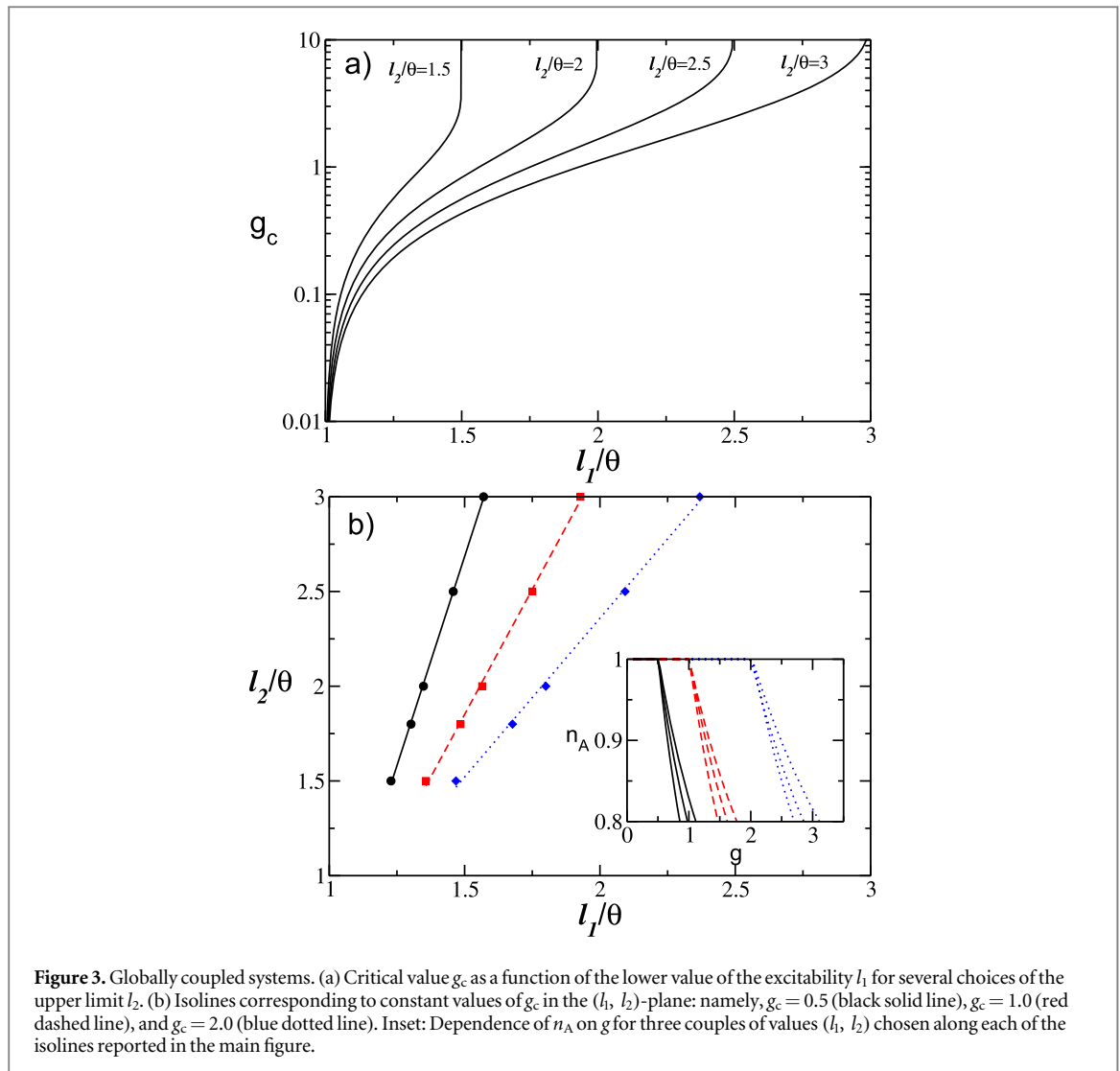$$g_c = (l_1 - \theta)/\bar{\nu}, \qquad (9)$$

Figure 3. Globally coupled systems. (a) Critical value g_c as a function of the lower value of the excitability l_1 for several choices of the upper limit l_2. (b) Isolines corresponding to constant values of g_c in the (l_1, l_2)-plane: namely, $g_c = 0.5$ (black solid line), $g_c = 1.0$ (red dashed line), and $g_c = 2.0$ (blue dotted line). Inset: Dependence of n_A on g for three couples of values (l_1, l_2) chosen along each of the isolines reported in the main figure.

and thus, for $l_1 = \theta$ even an infinitesimally small coupling is in principle sufficient to silence some neurons. Furthermore, from figure 3(a) it is evident that whenever the excitabilities become homogeneous, i.e. for $l_1 \rightarrow l_2$, the critical synaptic coupling g_c diverges toward infinity. Thus, heterogeneity in the excitability distribution is a necessary condition in order to observe a gradual neuronal death, as shown in figure 2(a).

This is in agreement with the results reported in [7], where homogeneous fully coupled networks of inhibitory LIF neurons have been examined. In particular, for finite systems and slow synapses, the authors in [7] revealed the existence of a sub-critical Hopf bifurcation from a fully synchronized state to a regime characterized by oscillator death occurring at some critical g_c. However, in the thermodynamic limit $g_c \rightarrow \infty$ for fast as well as slow synapses, which is in agreement with our mean field result for instantaneous synapses.

We also proceed to investigate the isolines corresponding to the same critical g_c in the (l_1, l_2)-plane, and the results are reported in figure 3(b) for three selected values of g_c. It is evident that the l_1 and l_2-values associated with the isolines display a direct proportionality among them. However, despite lying on the same g_c-isoline, different parameter values induce a completely different behavior of n_A as a function of the synaptic strength, as shown in the inset of figure 3(b).

Direct simulations of the network at finite sizes, namely for $N = 400$ and $N = 1400$, show that sufficiently large coupling neurons with similar excitabilities tend to form clusters, similarly to what was reported in [42], but with a delayed pulse transmission. However, in contrast to [42], the overall macroscopic dynamics is asynchronous, and no collective oscillations can be detected for the whole range of considered synaptic strengths.

4. Sparse networks: neuronal rebirth

In this section we will consider a network with sparse connectivity, namely each neuron is supra-threshold and it receives instantaneous IPSPs from $K \ll N$ randomly chosen neurons in the network. Due to the sparseness, the

input spike trains can be considered as uncorrelated, and at a first approximation it can be assumed that each spike train is Poissonian with a frequency $\bar{\nu}$ corresponding to the average firing rate of the neurons in the network [8, 9]. Usually, the mean activity of a LIF neural network is estimated in the context of the diffusion approximation [69, 80]. This approximation is valid whenever the arrival frequency of the IPSPs is high with respect to the firing emission, while the amplitude of each IPSPs (namely, $G = g/K$) is small with respect to the firing threshold θ. This latter hypothesis in our case is not valid for sufficiently large (small) synaptic strength g (in-degree K), as can be appreciated by the comparison shown in figure 13 in appendix B. Therefore, the synaptic inputs should be treated as shot noise. In particular, here we apply an extended version of the analytic approach derived by Richardson and Swabrick in [70] to estimate the average firing rate and the average coefficient of variation for LIF neurons with instantaneous synapses subject to inhibitory shot noise of constant amplitude (for more details see appendices B and C).

Contrasting with the fully coupled case, the fraction of active neurons n_A does not saturate to a constant value for sufficiently short times. Instead, n_A increases in time due to the rebirth of losers previously silenced by the firing activity of winners, as shown in figure 1(b). This effect is clearly illustrated by considering the probability distributions $P(\nu)$ of the firing rates of the neurons at successive integration times t_S. These are reported in the insets of figure 1(b) for two coupling strengths and two times: namely, $t_S = 985$ (red lines) and $t_S = 1 \times 10^6$ (green lines). From these data is evident that the fraction of neurons with low firing rate (the losers) increases with time, while the fraction of high firing neurons remains almost unchanged. Moreover, the variation of n_A slows down for increasing t_S, and n_A approaches some apparently asymptotic profile for sufficiently long integration times. Furthermore, n_A has a non-monotonic behavior with g, which is opposite to the fully coupled case. In particular, n_A reveals a minimum n_{A_m} at some intermediate synaptic strength g_m followed by an increase toward $n_A = 1$ at large g. As we have verified, as long as $1 < K \ll N$, finite size effects are negligible and the actual value of n_A depends only on the in-degree K and the considered simulation time t_S. In the following we will try to explain the origin of such a behavior.

Despite the model being fully deterministic, due to the random connectivity the rebirth of silent neurons can be interpreted in the framework of activation processes induced by random fluctuations. In particular, we can assume that each neuron in the network will receive $n_A K$ independent Poissonian trains of inhibitory kicks of constant amplitude G characterized by an average frequency $\bar{\nu}$; thus, each synaptic input can be regarded as a single Poissonian train with total frequency $R = n_A K \bar{\nu}$. Therefore, each neuron, characterized by its own excitability I, will be subject to an average effective input $\mu(I)$ (as reported in equation (4)) plus fluctuations in the synaptic current of intensity
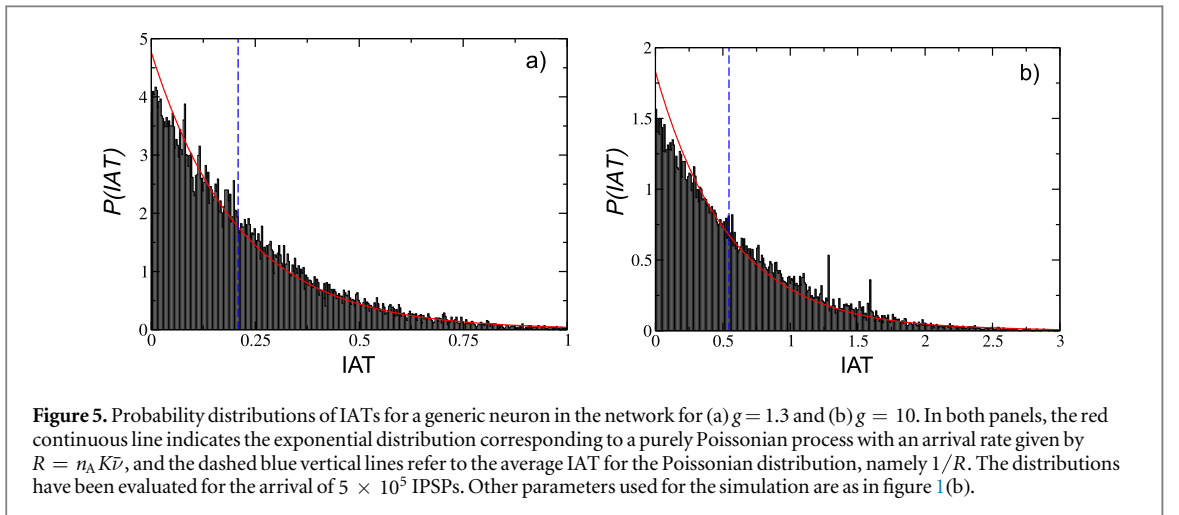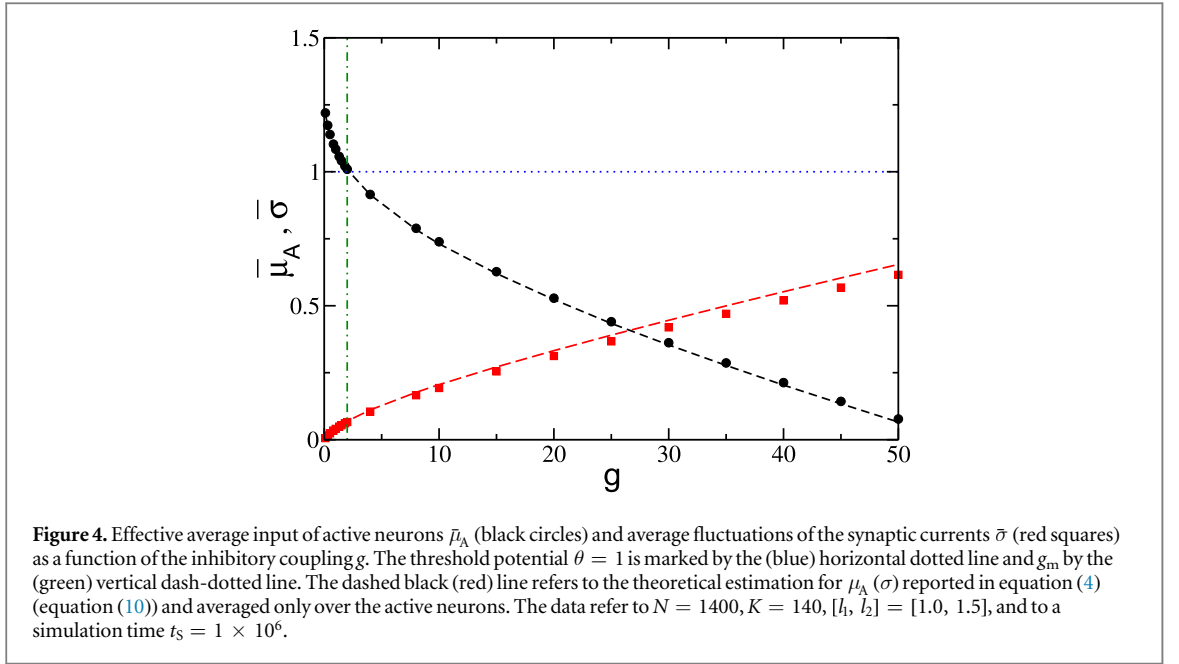
$$\sigma = g\sqrt{\frac{n_A \bar{\nu}}{K}}. \tag{10}$$

Indeed, we have verified that (10) gives a quantitatively correct estimation of the synaptic current fluctuations over the whole range of synaptic coupling considered (as shown in figure 4). A closer analysis of the probability distributions $P(IAT)$ of the inter-arrival times (IATs) reveals that these are essentially exponentially distributed, as expected for Poissonian processes, with a decay rate given by R, as evident from figure 5 for two different synaptic strengths. However, all these indications are not sufficient to guarantee that the IAT statistics are indeed Poissonian. In particular, as pointed out in [40], a superposition of uncorrelated spike trains generated by the same non-Poissonian renewal process can result in a peculiar non-renewal process characterized by exponentially distributed and uncorrelated IATs with a non-flat power spectrum. In our case we have indeed verified that for small coupling the power spectrum associated with the IATs deviates from the flat one at low frequencies, which is similar to the results reported in [40]; meanwhile, at large g the spectrum recovers a Poissonian shape. Therefore the hypothesis that the neuronal input is Poissonian in our case should be considered only as a first-order approximation, in particular for small synaptic couplings.

For instantaneous IPSP, the current fluctuations are due to stable chaos [63] since the maximal Lyapunov exponent is negative for the whole range of coupling, as we have verified. Therefore, as reported by many authors, erratic fluctuations in inhibitory neural networks with instantaneous synapses are due to finite amplitude instabilities, while at the infinitesimal level the system is stable [3, 29, 30, 42, 49, 82, 90].

In this circumstance, the silent neurons stay in a quiescent state corresponding to the minimum of the effective potential $\mathcal{U}(v) = v^2/2 - \mu v$, and in order to fire they should overcome a barrier $\Delta \mathcal{U} = (\theta - \mu)^2/2$. The average time t_A required to overcome such a barrier can be estimated accordingly to the Kramers' theory for activation processes [25, 80], namely

$$t_A \simeq \tau_0 \exp\left(\frac{(\theta - \mu(I))^2}{\sigma^2}\right), \tag{11}$$

where τ_0 is an effective time scale taking in account the intrinsic non-stationarity of the process, i.e. the fact that the number of active neurons increases during the time evolution.
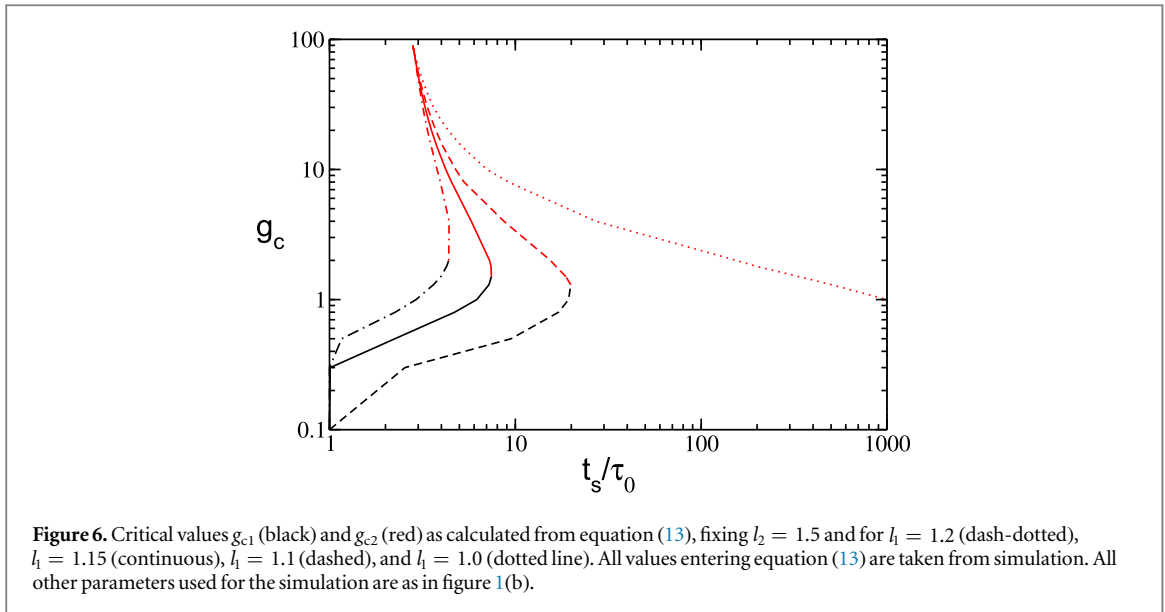
Figure 4. Effective average input of active neurons $\bar{\mu}_A$ (black circles) and average fluctuations of the synaptic currents $\bar{\sigma}$ (red squares) as a function of the inhibitory coupling g. The threshold potential $\theta = 1$ is marked by the (blue) horizontal dotted line and g_m by the (green) vertical dash-dotted line. The dashed black (red) line refers to the theoretical estimation for μ_A (σ) reported in equation (4) (equation (10)) and averaged only over the active neurons. The data refer to $N = 1400, K = 140, [l_1, l_2] = [1.0, 1.5]$, and to a simulation time $t_S = 1 \times 10^6$.

Figure 5. Probability distributions of IATs for a generic neuron in the network for (a) $g = 1.3$ and (b) $g = 10$. In both panels, the red continuous line indicates the exponential distribution corresponding to a purely Poissonian process with an arrival rate given by $R = n_A K \bar{\nu}$, and the dashed blue vertical lines refer to the average IAT for the Poissonian distribution, namely $1/R$. The distributions have been evaluated for the arrival of 5×10^5 IPSPs. Other parameters used for the simulation are as in figure 1(b).

It is important to stress that the expression (11) will remain valid also in the limit of large synaptic couplings, not only because of σ^2, but also because the barrier height will increase with g. Furthermore, both these quantities grow quadratically with g at sufficiently large synaptic strength, as it can be inferred from equations (4) and (10).

It is reasonable to assume that at a given time t_S all neurons with $t_A < t_S$ will have fired at least once, and that the more excitable will fire first. Therefore, by assuming that the fraction of active neurons at time t_S is $n_A(t_S)$, the last neuron that has fired should be characterized by the following excitability:

$$\hat{I} = l_2 - n_A(t_S)(l_2 - l_1). \tag{12}$$

Here, excitabilities I are uniformly distributed in the interval $[l_1, l_2]$. In order to obtain an explicit expression for the fraction of active neurons at time t_S, one should solve the equation (11) for the neuron with excitability $\hat{I}$ by setting $t_S = t_A$, thus obtaining the following solution

$$n_A(t_S) = \begin{cases} \dfrac{\phi - 2\beta\gamma + \sqrt{\phi^2 - 4\phi\beta\gamma}}{2\gamma^2} & \text{if } n_A < 1 \\ 1 & \text{otherwise} \end{cases} \tag{13}$$

Figure 6. Critical values g_{c1} (black) and g_{c2} (red) as calculated from equation (13), fixing $l_2 = 1.5$ and for $l_1 = 1.2$ (dash-dotted), $l_1 = 1.15$ (continuous), $l_1 = 1.1$ (dashed), and $l_1 = 1.0$ (dotted line). All values entering equation (13) are taken from simulation. All other parameters used for the simulation are as in figure 1(b).

where

$$\gamma = (l_2 - l_1) + g\bar{\nu} \quad \phi = \frac{g^2}{K}\bar{\nu}\ln(t_S/\tau_0) \quad \beta = \theta - l_2.$$

Equation (13) gives the dependence of n_A on the coupling strength g for a fixed integration time t_S and time scale τ_0 whenever we can provide the value of the average frequency $\bar{\nu}$. A quick inspection of equations (11) and (13) shows that, setting $n_A = 1$, we obtain two solutions for the critical couplings g_{c1} (g_{c2}) below (above) that all neurons will fire at least once in the considered time interval. The solutions are reported in figure 6. In particular, we observe that whenever $l_1 \to \theta$ the critical coupling g_{c1} will vanish, which is analogous to the fully coupled situation. These results clearly indicate that n_A should display a minimum for some finite coupling strength $g_m \in (g_{c1}, g_{c2})$. Furthermore, as shown in figure 6 the two critical couplings approach one another for increasing t_S and finally merge, indicating that at sufficiently long times all neurons will be active at any synaptic coupling strength g.
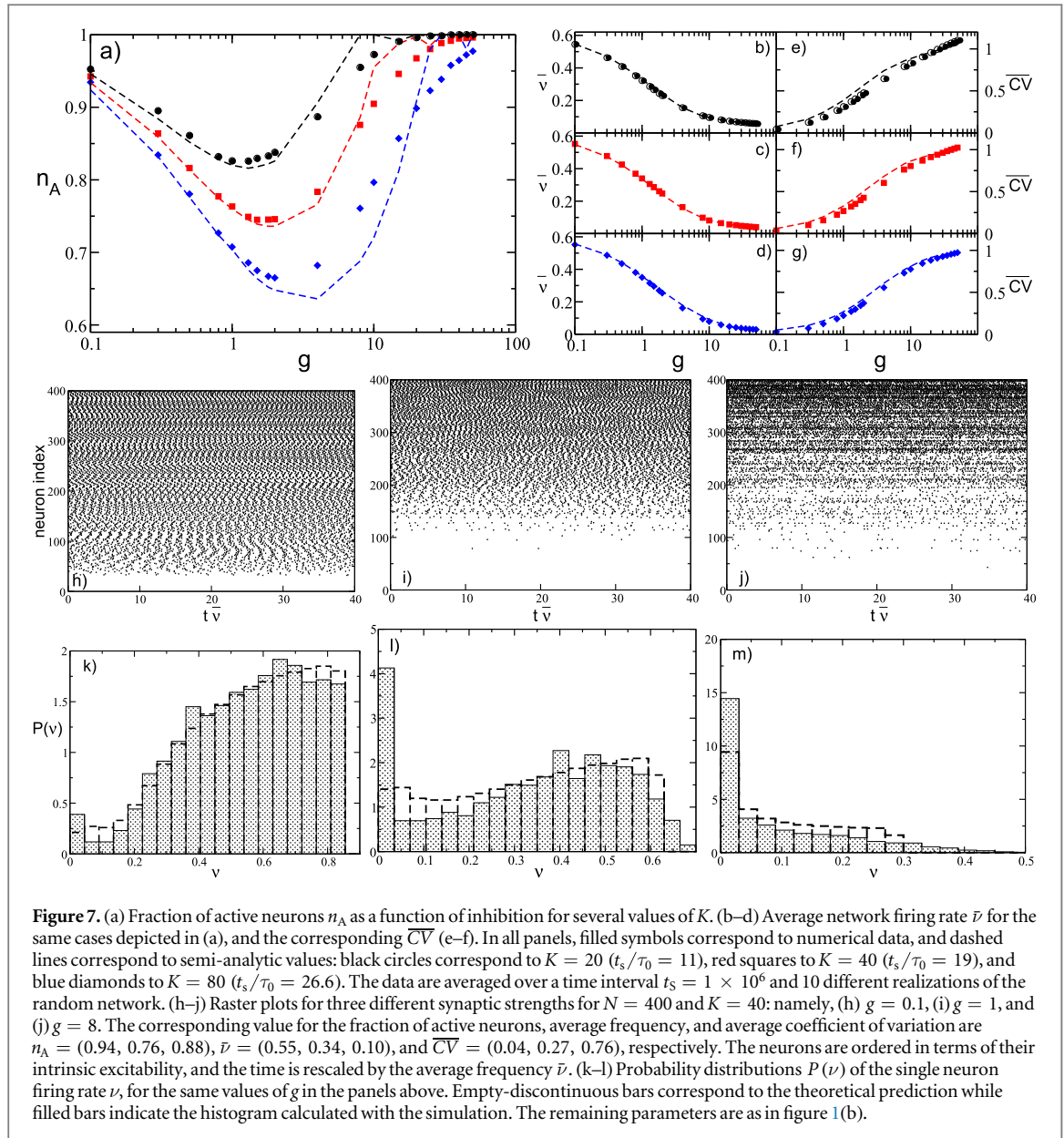
The average frequency $\bar{\nu}$ can be obtained analytically by following the approach described in appendix B for LIF neurons with instantaneous synapses subject to inhibitory Poissonian spike trains. In particular, the self-consistent expression for the average frequency reads as

$$\bar{\nu} = \int_{\{I_A\}} dI\, P(I)\nu_0(I, G, n_A, \bar{\nu}), \tag{14}$$

where the explicit expression of ν_0 is given by equation (31) in appendix B.

The simultaneous solution of equations (13) and (14) provides a theoretical estimation of n_A and $\bar{\nu}$ for the whole considered range of synaptic strength, once the unknown time scale τ_0 is fixed. This time scale has been determined via an optimal fitting procedure for sparse networks with $N = 400$ and $K = 20, 40$, and 80 at a fixed integration time $t_S = 1 \times 10^6$. The results for n_A are reported in figure 7(a). The estimated curves reproduce reasonably well the numerical data for $K = 20$ and 40, while for $K = 80$ the agreement worsens at large coupling strengths. This could be due to the fact that by increasing g and K, the spike trains stimulating each neuron cannot be assumed to be completely independent, as done for the derivation of equations (13) and (14). Nevertheless, the average frequency $\bar{\nu}$ is quantitatively well reproduced for the considered K values over the entire range of synaptic strengths, as is evident from figures 7(b)–(d). A more detailed comparison between the theoretical estimations and the numerical data can be obtained by considering the distributions $P(\nu)$ of the single neuron firing rate for different coupling strengths reported in figures 7(k)–(m) for $K = 40$. The overall agreement can be considered as more than satisfactory, while observable discrepancies are probably due to the fact that our approach neglected a further source of disorder present in the system and related to heterogeneity in the number of active pre-synaptic neurons [9].

We have also analytically estimated the average coefficient of variation of the firing neurons $\overline{CV}$ by extending the method derived in [70] to obtain the response of a neuron receiving synaptic shot noise input. The analytic expressions of the coefficient of variation for LIF neurons subject to inhibitory shot noise with fixed post-synaptic amplitude are obtained by estimating the second moment of the associated first-passage-time distribution; the details are reported in appendix C. The coefficient of variation can be estimated once the self-

Figure 7. (a) Fraction of active neurons n_A as a function of inhibition for several values of K. (b–d) Average network firing rate $\bar{\nu}$ for the same cases depicted in (a), and the corresponding $\overline{CV}$ (e–f). In all panels, filled symbols correspond to numerical data, and dashed lines correspond to semi-analytic values: black circles correspond to $K = 20$ ($t_s/\tau_0 = 11$), red squares to $K = 40$ ($t_s/\tau_0 = 19$), and blue diamonds to $K = 80$ ($t_s/\tau_0 = 26.6$). The data are averaged over a time interval $t_s = 1 \times 10^6$ and 10 different realizations of the random network. (h–j) Raster plots for three different synaptic strengths for $N = 400$ and $K = 40$: namely, (h) $g = 0.1$, (i) $g = 1$, and (j) $g = 8$. The corresponding value for the fraction of active neurons, average frequency, and average coefficient of variation are $n_A = (0.94, 0.76, 0.88)$, $\bar{\nu} = (0.55, 0.34, 0.10)$, and $\overline{CV} = (0.04, 0.27, 0.76)$, respectively. The neurons are ordered in terms of their intrinsic excitability, and the time is rescaled by the average frequency $\bar{\nu}$. (k–l) Probability distributions $P(\nu)$ of the single neuron firing rate ν, for the same values of g in the panels above. Empty-discontinuous bars correspond to the theoretical prediction while filled bars indicate the histogram calculated with the simulation. The remaining parameters are as in figure 1(b).

consistent values for n_A and $\bar{\nu}$ have been obtained via equations (13) and (14). The comparison with the numerical data, reported in figures 7(e)–(g), reveals a good agreement over the whole range of synaptic strengths for all considered in-degrees.

At sufficiently small synaptic coupling the neurons fire tonically and almost independently, as shown by the raster plot in figure 7(h) and by the fact that $\bar{\nu}$ approaches the average value for the uncoupled system (namely, 0.605) and $\overline{CV} \to 0$. Furthermore, the neuronal firing rates are distributed toward finite values, indicating that the inhibition has a minor role in this case, as shown in figure 7(k). By increasing the coupling, n_A decreases, and as an effect of the inhibition more and more neurons are silenced (as evident from figure 7(l)) and the average firing rate decreases; at the same time, the dynamics become slightly more irregular, as shown in figure 7(i). At large coupling $g > g_m$, a new regime appears, where almost all neurons become active but with extremely slow dynamics that are essentially stochastic with $\overline{CV} \simeq 1$, as also testified by the raster plot reported in figure 7(j) and by the firing rate distribution shown in figure 7(m).

Furthermore, from figure 7(a) it is clear that the minimum value of the fraction of active neurons n_{A_m} decreases by increasing the network in-degree K, while g_m increases with K. This behavior is further investigated in a larger network, namely $N = 1400$, and reported in the inset of figure 8. It is evident that n_A stays close to the globally coupled solutions over larger and larger intervals for increasing K. This can be qualitatively understood by the fact that the current fluctuations in equation (10), responsible for the rebirth of silent neurons, are proportional to g and scales as $1/\sqrt{K}$. Therefore, at larger in-degrees the fluctuations have similar intensities only for larger synaptic coupling.
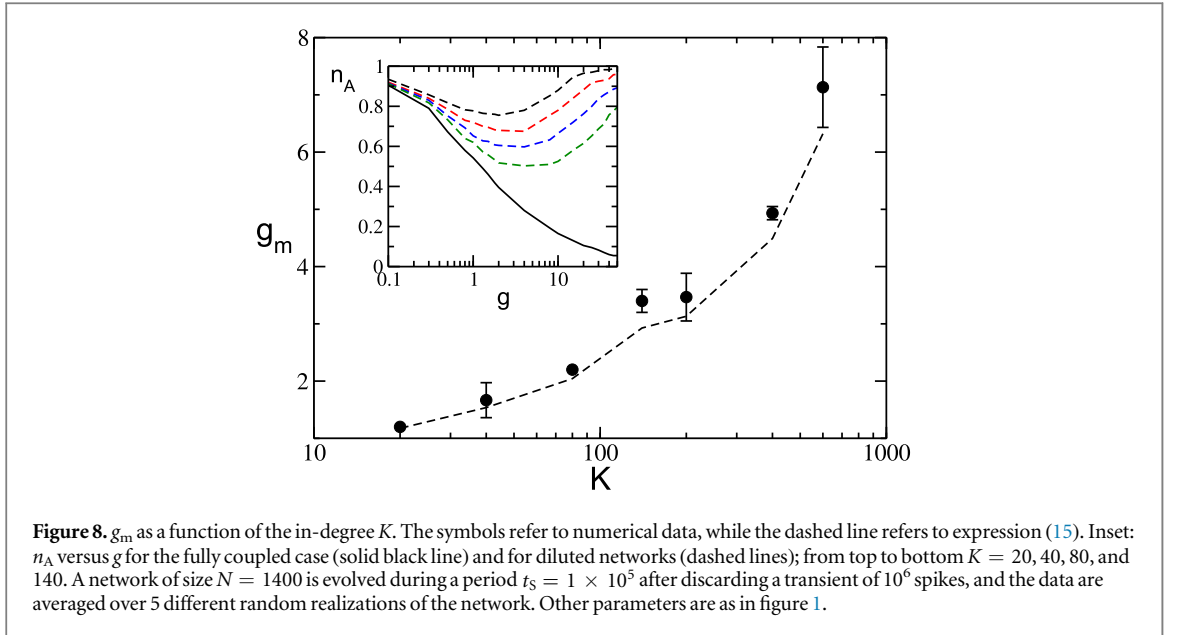
Figure 8. g_m as a function of the in-degree K. The symbols refer to numerical data, while the dashed line refers to expression (15). Inset: n_A versus g for the fully coupled case (solid black line) and for diluted networks (dashed lines); from top to bottom $K = 20, 40, 80,$ and 140. A network of size $N = 1400$ is evolved during a period $t_S = 1 \times 10^5$ after discarding a transient of 10^6 spikes, and the data are averaged over 5 different random realizations of the network. Other parameters are as in figure 1.

The general mechanism behind neuronal rebirth can be understood by considering the values of the effective neuronal input and current fluctuations as a function of g. As shown in figure 4, the effective input current $\bar{\mu}_A$, averaged over the active neurons, essentially coincides with the average excitability $\bar{I}_A$ for $g \to 0$, where the neurons can be considered as independent from others. The inhibition leads to a decrease of $\bar{\mu}_A$, and to a crossing of the threshold θ at exactly $g = g_m$. This indicates that at $g < g_m$ the active neurons, being on average supra-threshold, fire almost tonically inhibiting the losers via a WTA mechanism. In this case the firing neurons are essentially mean-driven and the current fluctuations play a role in the rebirth of silent neurons only on extremely long time scales; this is confirmed by the low values of $\bar{\sigma}$ in such a range, as evident from figure 4. On the other hand, for $g > g_m$, the active neurons are now on average below threshold while fluctuations dominate dynamics. In particular, the firing is now extremely irregular mainly due to re-activation processes. Therefore, the origin of the minimum in n_A can be understood as a transition from a mean-driven to a fluctuation-driven regime [68].

A quantitative definition of g_m can be given by requiring that the average input current of the active neurons $\bar{\mu}_A$ crosses the threshold θ at $g = g_m$, namely

$$\bar{\mu}_A (g_m) = \bar{I}_A - g_m \bar{\nu}_m n_{A_m} = \theta,$$
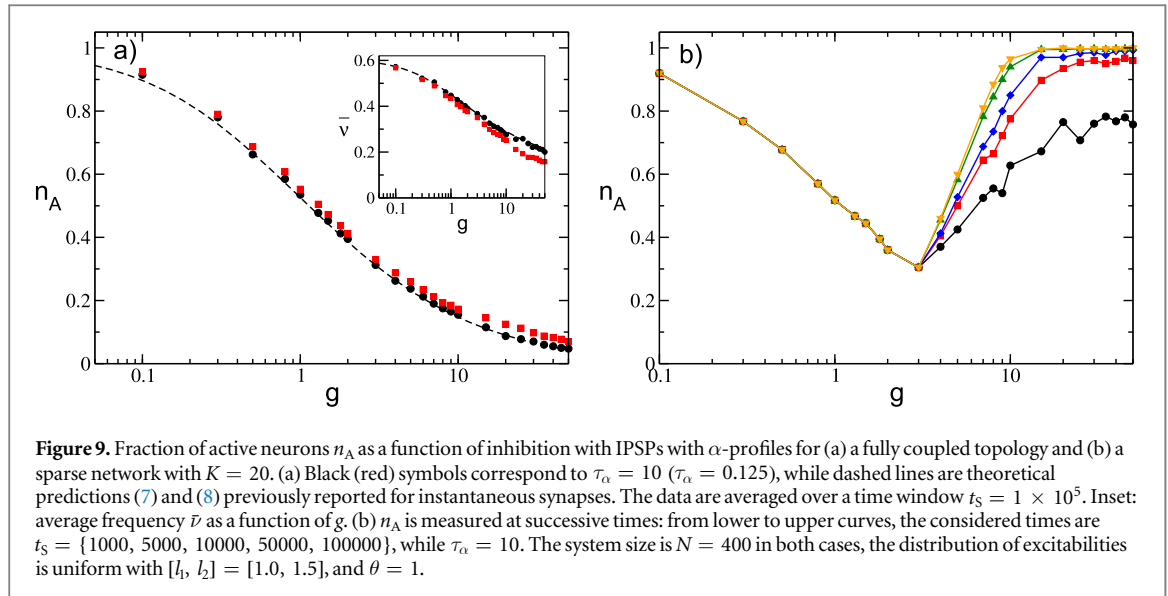
where $\bar{I}_A$ is the average excitability of the firing neurons, while n_{A_m} and $\bar{\nu}_m$ are the fraction of active neurons and the average frequency at the minimum.

For a uniform distribution $P(I)$, a simpler expression for g_m can be derived, namely

$$g_m = \bar{\nu}_m^{-1} \left[\frac{l_2 - \theta}{n_{A_m}} + \frac{1}{2}(l_1 - l_2) \right]. \tag{15}$$

We have compared the numerical measurements of g_m with the estimations obtained by employing equation (15), where n_{A_m} and $\bar{\nu}$ are obtained from the simulations. As shown in figure 8, for a network of size $N = 1400$, the overall agreement is more than satisfactory for in-degrees ranging over almost two decades (namely, for $20 \leqslant K \leqslant 600$). This confirms that our guess (that the minimum n_{A_m} occurs exactly at the transition from mean-driven to fluctuation-driven dynamics) is consistent with the numerical data for a wide range of in-degrees.

It should be stressed that, as we have verified for various system sizes (namely, $N = 700, 1400,$ and 2800) and for a constant average in-degree $K = 140$, for instantaneous synapses the network is in an heterogeneous asynchronous state for all considered values of synaptic coupling. This is demonstrated by the fact that the intensity of the fluctuations of average firing activity, measured by considering the low-pass filtered linear superposition of all the spikes emitted in the network, vanishes as $1/\sqrt{N}$ [85]. Therefore, the observed transition at $g = g_m$ is not associated with the emergence of irregular collective behaviors as reported for globally coupled heterogeneous inhibitory networks of LIF neurons with delay [42] or pulse-coupled phase oscillators [82].

Figure 9. Fraction of active neurons n_A as a function of inhibition with IPSPs with α-profiles for (a) a fully coupled topology and (b) a sparse network with $K = 20$. (a) Black (red) symbols correspond to $\tau_\alpha = 10$ ($\tau_\alpha = 0.125$), while dashed lines are theoretical predictions (7) and (8) previously reported for instantaneous synapses. The data are averaged over a time window $t_S = 1 \times 10^5$. Inset: average frequency $\bar{\nu}$ as a function of g. (b) n_A is measured at successive times: from lower to upper curves, the considered times are $t_S = \{1000, 5000, 10000, 50000, 100000\}$, while $\tau_\alpha = 10$. The system size is $N = 400$ in both cases, the distribution of excitabilities is uniform with $[l_1, l_2] = [1.0, 1.5]$, and $\theta = 1$.

5. Effect of synaptic filtering

In this section we will investigate how synaptic filtering can influence the previously reported results. In particular, we will consider non-instantaneous IPSP with an α-function profile (3), whose evolution is ruled by a single time scale τ_α.

5.1. Fully coupled networks

Let us first examine the fully coupled topology. In this case we analogously observe the δ-pulse coupling by increasing the inhibition so that the number of active neurons steadily decreases toward a limit where only few neurons (or eventually only one) will survive. At the same time the average frequency also decreases monotonically, as shown in figure 9 for two different τ_α differing by almost two orders of magnitude. Furthermore, the mean field estimations (7) and (8) obtained for n_A and $\bar{\nu}$ represent a very good approximation for α-pulses (as shown in figure 9). In particular, the mean field estimation essentially coincides with the numerical values for slow synapses, as evident from the data reported in figure 9 for $\tau_\alpha = 10$ (black filled circles). This can be explained by the fact that for sufficiently slow synapses, with $\tau_P > \bar{T}_{ISI}$, the neurons feel the synaptic input current as continuous because each input pulse has essentially no time to decay between two firing events. Therefore, the mean field approximation for the input current (4) works well in this case. This is particularly true for $\tau_\alpha = 10$, where $\tau_P = 20$ and $\bar{T}_{ISI} \simeq 2 - 6$ in the range of the considered coupling. While for $\tau_\alpha = 0.125$, we observe some deviation from the mean field results (red squares in figure 9). The reason for these discrepancies resides in the fact that $\tau_P < \bar{T}_{ISI}$ for any coupling strength, and therefore the discreteness of the pulses cannot be completely neglected, particularly for large amplitudes (large synaptic couplings). This is analogous to what is observed for instantaneous synapses.

5.2. Sparse networks

For sparse networks, n_A has the same qualitative behavior as a function of the synaptic inhibition observed for instantaneous IPSPs, as shown in figure 9(b) and figure 10(a). The value of n_A decreases with g and reaches a minimal value at g_m; afterwards, it increases towards $n_A = 1$ at larger coupling. The origin of the minimum of n_A as a function of g is the same as for instantaneous synapses. For $g < g_m$, active neurons are subject to, on average, a supra-threshold effective input $\bar{\mu}_A$ while at larger coupling $\bar{\mu}_A < \theta$, as shown in the inset of figure 10(b). This is true for any value of τ_α; however, this transition from mean- to fluctuation-driven dynamics becomes dramatic for slow synapses. As evidenced from the data for the average output firing rate $\bar{\nu}$ and the average coefficient of variation $\overline{CV}$, these quantities have almost discontinuous jumps at $g = g_m$, as shown in figure 11.

Therefore, let us first concentrate on slow synapses with τ_α larger than the membrane time constant, which is one for adimensional units. For $g < g_m$ the fraction of active neurons is frozen in time, at least on the considered time scales, as revealed by the data in figure 9(b). Furthermore, for $g < g_m$, the mean field approximation obtained for the fully coupled case works almost perfectly both for n_A and $\bar{\nu}$, as reported in figure 10(a). The frozen phase is characterized by extremely small values of current fluctuations $\bar{\sigma}$ (as shown figure 10(b)) and a quite high firing rate $\bar{\nu} \simeq 0.4 - 0.5$ with an associated average coefficient of variation $\overline{CV}$ of almost zero (see black circles and red squares in figure 11). Instead, for $g > g_m$ the number of active neurons increases in time
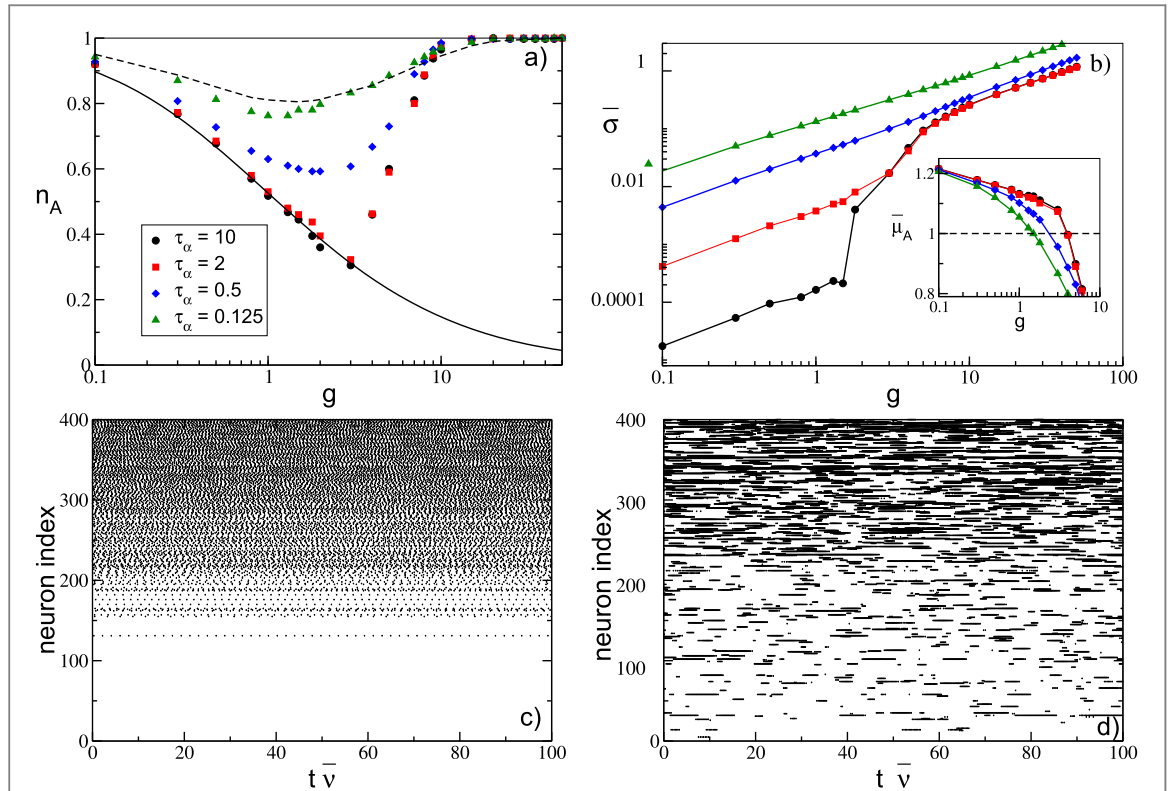
Figure 10. (a) Fraction of active neurons for a network of α-pulse-coupled neurons as a function of g for various τ_α: namely, $\tau_\alpha = 10$ (black circles), $\tau_\alpha = 2$ (red squares), $\tau_\alpha = 0.5$ (blue diamonds), and $\tau_\alpha = 0.125$ (green triangles). For instantaneous synapses, the fully coupled analytic solution is reported (solid line), as well as the measured n_A for the sparse network with same level of dilution and estimated over the same time interval (dashed line). (b) Average fluctuations of the synaptic current $\bar{\sigma}$ versus g for ISPSs with α-profiles; the symbols refer to the same τ_α as in panel (a). Inset: Average input current $\bar{\mu}_A$ of the active neurons versus g, where the dashed line is the threshold value $\theta = 1$. The simulation time has been fixed to $t_S = 1 \times 10^5$. (c–d) Raster plots for two different synaptic strengths for $\tau_\alpha = 10$: namely, (c) $g = 1$ corresponds to $n_A \simeq 0.52$, $\bar{\nu} \simeq 0.45$, and $\overline{CV} \simeq 3 \times 10^{-4}$; while (i) $g = 10$ to $n_A \simeq 0.99$, $\bar{\nu} \simeq 0.06$, and $\overline{CV} \simeq 4.1$. The neurons are ordered according to their intrinsic excitability and the time is rescaled by the average frequency $\bar{\nu}$. The data were obtained for a system size $N = 400$ and $K = 20$, and other parameters are as in figure 9.
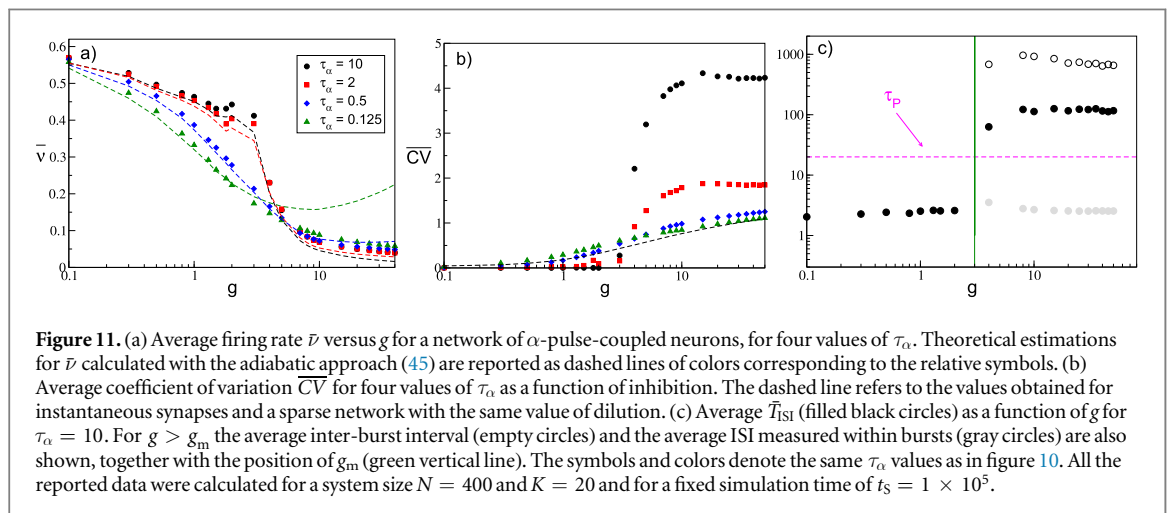
Figure 11. (a) Average firing rate $\bar{\nu}$ versus g for a network of α-pulse-coupled neurons, for four values of τ_α. Theoretical estimations for $\bar{\nu}$ calculated with the adiabatic approach (45) are reported as dashed lines of colors corresponding to the relative symbols. (b) Average coefficient of variation $\overline{CV}$ for four values of τ_α as a function of inhibition. The dashed line refers to the values obtained for instantaneous synapses and a sparse network with the same value of dilution. (c) Average $\bar{T}_{ISI}$ (filled black circles) as a function of g for $\tau_\alpha = 10$. For $g > g_m$ the average inter-burst interval (empty circles) and the average ISI measured within bursts (gray circles) are also shown, together with the position of g_m (green vertical line). The symbols and colors denote the same τ_α values as in figure 10. All the reported data were calculated for a system size $N = 400$ and $K = 20$ and for a fixed simulation time of $t_S = 1 \times 10^5$.

similarly to what is observed for instantaneous synapses, while the average frequency becomes extremely small $\bar{\nu} \simeq 0.04 - 0.09$ and the value of the coefficient of variation becomes definitely larger than one.

These effects can be explained by the fact that below g_m the active neurons (the winners) are subject to an effective input $\bar{\mu}_A > \theta$ that induces a quite regular firing, as testified by the raster plot displayed in figure 10(c). The supra-threshold activity of the winners joined together with the filtering action of the synapses guarantee that on average each neuron in the network receives an almost continuous current with small fluctuations in time. These results explain why the mean field approximation still works in the frozen phase, where fluctuations in synaptic currents are essentially negligible and unable to induce any neuronal rebirth, at least on realistic time

scales. In this regime the only mechanism in action is the WTA, and fluctuations begin to have a role for slow synapses only for $g > g_m$. Indeed, as shown in figure 10(b), the synaptic fluctuations $\bar{\sigma}$ for $\tau_\alpha = 10$ (black circles) are almost negligible for $g < g_m$ and show an enormous increase of almost two orders of magnitude at $g = g_m$. Similarly, at $\tau_\alpha = 2$ (red square) a noticeable increase of $\bar{\sigma}$ is observable at the transition.
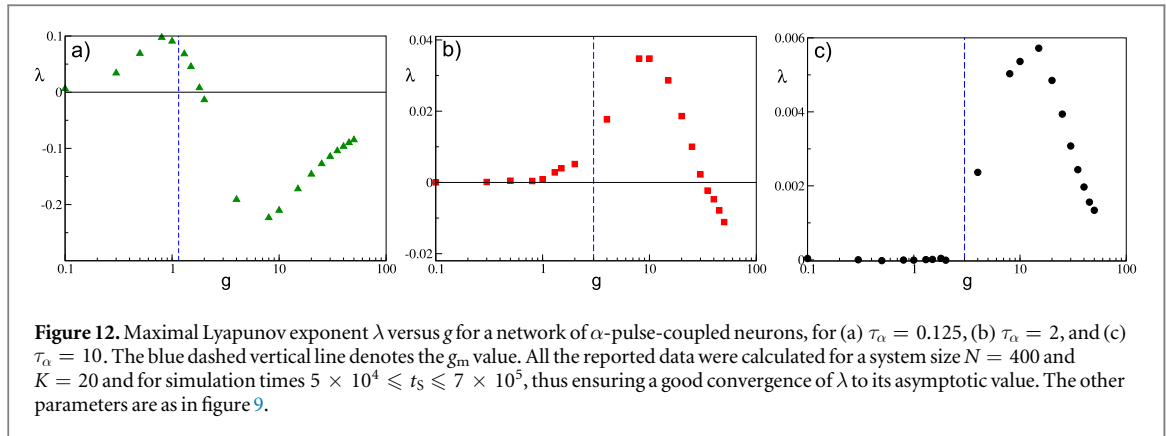
In order to better understand the abrupt changes in $\bar{\nu}$ and $\overline{CV}$ observable for slow synapses at $g = g_m$, let us consider the case $\tau_\alpha = 10$. As shown in figure 11(c), $\tau_P > \bar{T}_{ISI} \simeq 2 - 3$ for $g < g_m$. Therefore, for these couplings the IPSPs have no time to decay between a firing emission and the next one, and thus the synaptic fluctuations $\bar{\sigma}$ are definitely small in this case. At g_m an abrupt jump is observable to large values where $\bar{T}_{ISI} > \tau_P$, which is due to the fact that now the neurons display bursting activities, as evident from the raster plot shown in figure 10(d). The bursting is due to the fact that, for $g > g_m$, the active neurons are subject to an effective input, which is on average sub-threshold; therefore, the neurons tend to be silent. However, due to current fluctuations, a neuron can pass the threshold and silent periods can be interrupted by bursting phases where the neuron fires almost regularly. In fact, the silent (inter-burst) periods are very long $\simeq 700 - 900$ compared to the duration of the bursting periods, namely $\simeq 25 - 50$, as shown in figure 11(c). This explains the abrupt decrease of the average firing rate reported in figure 11(a). Furthermore, the inter-burst periods are exponentially distributed with an associated coefficient of variation $\simeq 0.8 - 1.0$, which clearly indicates the stochastic nature of the switching from the silent phase to the bursting phase. The firing periods within the bursting phase are instead quite regular, with an associated coefficient of variation $\simeq 0.2$, and with a duration similar to $\bar{T}_{ISI}$ measured in the frozen phase (shaded gray circles in figure 11(c)). Therefore, above g_m the distribution of the ISI exhibits a long exponential tail associated with the bursting activity, and this explains the very large values of the measured coefficient of variation. By increasing coupling, the fluctuations in the input current become larger, and thus the fraction of neurons that fires at least once within a certain time interval increases. At the same time, $\bar{\nu}$, the average inter-burst periods, and the firing periods within the bursting phase remain almost constant at $g > 10$, as shown in figure 11(a). This indicates that the decrease of $\bar{\mu}_A$ and increase of $\bar{\sigma}$ due to the increased inhibitory coupling essentially compensate for each other in this range. Indeed, we have verified that for $\tau_\alpha = 10$ and $\tau_\alpha = 2$, $\bar{\mu}_A$ ($\bar{\sigma}$) decreases (increases) linearly with g with similar slopes, namely $\bar{\mu}_A \simeq 0.88 - 0.029g$ while $\bar{\sigma} \simeq 0.05 + 0.023g$.

For faster synapses, the frozen phase is no longer present. Furthermore, due to rebirths induced by current fluctuations, n_A is always larger than the fully coupled mean field result (8), even at $g < g_m$. It is interesting to notice that by decreasing τ_α, we are now approaching the instantaneous limit, as indicated by the results reported for n_A in figure 10(a) and $\overline{CV}$ in figure 11(b). In particular, for $\tau_\alpha = 0.125$ (green triangles) the data almost collapses on the corresponding values measured for instantaneous synapses in a sparse network with the same characteristics and over a similar time interval (dashed line). Furthermore, for fast synapses with $\tau_\alpha < 1$ the bursting activity is no longer present, as can be appreciated by the fact that at most $\overline{CV}$ approaches one in the very large coupling limit.

For sufficiently slow synapses, the average firing rate $\bar{\nu}$ can be estimated by applying the so-called adiabatic approach developed by Moreno-Bote and Parga in [50, 51]. This method applies to LIF neurons with a synaptic time scale longer than the membrane time constant. In these conditions, the output firing rate can be reproduced by assuming that the neuron is subject to an input current with time-correlated fluctuations, which can be represented as colored noise with a correlation time given by the pulse duration $\tau_P = 2\tau_\alpha$ (for more details see appendix D). In this case we are unable to develop a self-consistent approach to obtain at the same time n_A and the average frequency. However, once n_A is provided by simulations, the estimated solution to (45) obtained with the adiabatic approach gives very good agreement with the numerical data for sufficiently slow synapses, namely for $\tau_P \geqslant 1$, as shown in figure 11(a) for $\tau_\alpha = 10, 2$, and 0.5. The theoretical expression (45) is even able to reproduce the jump in average frequencies observable at g_m, and can therefore capture the bursting phenomenon. By considering $\tau_P < 1$, as expected, the theoretical expression fails to reproduce the numerical data, particularly at large coupling (see the dashed green line in figure 11(a) corresponding to $\tau_\alpha = 0.125$).

By following the arguments reported in [50], the bursting phenomenon observed for $\tau_\alpha > 1$ and $g > g_m$ can be interpreted at a mean field level as the response of a sub-threshold LIF neuron subject to colored noise with correlation τ_P. In this case, the neuron is definitely sub-threshold, but in the presence of a large fluctuation it can lead to firing, and due to the finite correlation time, it can remain supra-threshold regularly firing for a period $\simeq \tau_P$. The validity of this interpretation is confirmed by the fact that the measured average bursting periods are of the order of the correlation time $\tau_P = 2\tau_\alpha$, namely, $\simeq 27 - 50$ ($\simeq 7 - 14$) for $\tau_\alpha = 10$ ($\tau_\alpha = 2$).

As a final point, to better understand the dynamical origin of the measured fluctuations in this deterministic model, we have estimated the maximal Lyapunov exponent λ. As expected from previous analysis, for non-instantaneous synapses we can observe the emergence of regular chaos in purely inhibitory networks [1, 30, 89]. In particular, for sufficiently fast synapses, we typically note a transition from a chaotic state at low coupling to a linearly stable regime (with $\lambda < 0$) at large synaptic strengths, as shown in figure 12(a) for $\tau_\alpha = 0.125$. This is despite the fact that current fluctuations are monotonically increasing with synaptic strength. Therefore,

Figure 12. Maximal Lyapunov exponent λ versus g for a network of α-pulse-coupled neurons, for (a) $\tau_\alpha = 0.125$, (b) $\tau_\alpha = 2$, and (c) $\tau_\alpha = 10$. The blue dashed vertical line denotes the g_m value. All the reported data were calculated for a system size $N = 400$ and $K = 20$ and for simulation times $5 \times 10^4 \leqslant t_S \leqslant 7 \times 10^5$, thus ensuring a good convergence of λ to its asymptotic value. The other parameters are as in figure 9.

fluctuations are due to chaos at small coupling, while at larger g they are due to finite amplitude instabilities, as expected for stable chaotic systems [3]. However, the passage from positive to negative values of the maximal Lyapunov exponent is not related to the transition occurring at g_m from mean-driven to a fluctuation-driven dynamics in the network.

For slow synapses, λ is essentially zero at small coupling in the frozen phase, characterized by tonic spiking of the neurons, but becomes positive by approaching g_m. For larger synaptic strengths λ, after reaching a maximal value, it decreases and eventually becomes negative at $g \gg g_m$, as reported in figures 12(b)–(c). Only for extremely slow synapses, as shown in figure 12(c) for $\tau_\alpha = 10$, the chaos onset seems to coincide with the transition occurring at g_m. These findings are consistent with recent results concerning the emergence of asynchronous rate chaos in homogeneous inhibitory LIF networks with deterministic [26] and stochastic [31] evolution. However, a detailed analysis of this aspect goes beyond the scope of the present paper.

6. Discussion

In this paper we have shown that the effect reported in [1, 66] is observable whenever two sources of quenched disorder are present in the network: namely, a random distribution of neural properties and a random topology. In particular, we have shown that neuronal death due to synaptic inhibition is observable only for heterogeneous distributions of neural excitabilities. Furthermore, in a globally coupled network the less excitable neurons are silenced for increasing synaptic strength until only one or few neurons remain active. This scenario corresponds to the WTA mechanism via lateral inhibition, which has often been invoked in neuroscience to explain several brain functions [88]. WTA mechanisms have been proposed to model hippocampal CA1 activity [16], as well as to be at the basis of visual velocity estimates [24], and to be essential for controlling visual attention [28].

However, most brain circuits are characterized by sparse connectivity [10, 38, 60], and in these networks we have shown that an increase in inhibition can lead from a phase dominated by neuronal death to a regime where neuronal rebirths occur. Therefore, the growth of inhibition can have the counter-intuitive effect to activate silent neurons due to the enhancement of current fluctuations. The reported transition is characterized by a passage from a regime dominated by the almost tonic activity of a group of neurons, to a phase where sub-threshold fluctuations are at the origin of the irregular firing of a high number of neurons in the network. For instantaneous synapses, the first and second moment of the firing distributions have been obtained together with the fraction of active neurons using a mean field approach, where the neuronal rebirth is interpreted as an activation process driven by synaptic shot noise [70].

For a finite synaptic time smaller than the characteristic membrane time constant, the scenario is similar to that observed for instantaneous synapses. However, the transition from mean-driven to fluctuation-driven dynamics becomes dramatic for sufficiently slow synapses. In this situation one observes for low synaptic strength a frozen phase, where synaptic filtering washes out the current fluctuations, thus leading to extremely regular dynamics controlled only by a WTA mechanism. As soon as the inhibition is sufficiently strong to lead the active neurons below threshold, neuronal activity becomes extremely irregular, exhibiting long silent phases interrupted by bursting events. The origin of these bursting periods can be understood in terms of the emergence of correlations in current fluctuations induced by the slow synaptic time scale, as explained in [50].

In our model, the random dilution of network connectivity is a fundamental ingredient to generate current fluctuations, whose intensity is controlled by the average network in-degree K. A natural question is whether the reported scenario will remain observable in the thermodynamic limit. On the basis of previous studies we can affirm that this depends on how K scales with the system size [22, 41, 75]. In particular, if K stays finite for $N \to \infty$ the transition will remain observable. For K diverging with N, the fluctuations become negligible for

Table 1. Comparison between the results obtained for slow α-synapses and experimental data for MSNs. The numerical data refer to results obtained in the bursting phase, namely for synaptic strength g in the range [10: 50], for simulation times $t_S = 1 \times 10^5$, $N = 400$, and $K = 20$. The experimental data refer to MSNs population in the striatum of free behaving wild type mice [47].

τ_α/τ_m	τ_m (msec)	Spike rate (Hz)	$\overline{CV}$	Burst duration (msec)	Spike rate within bursts (Hz)
2	10	4–6	$\simeq 1.8$	100 ± 40	42 ± 2
	20	2–3	$\simeq 1.8$	200 ± 80	21 ± 1
10	10	4–6	$\simeq 4.2$	400 ± 150	41 ± 2
	20	2–3	$\simeq 4.2$	800 ± 300	20 ± 1
	Experimental data	2–3	$\simeq 1.5$–3	500–1100	31 ± 15

sufficiently large system sizes, impeding neuronal rebirths, and the dynamics will be controlled only by the WTA mechanism.

An additional source of randomness present in the network is related to the variability in the number of active pre-synaptic neurons. In our mean field approach we have assumed that each neuron is subject to $n_A K$ spike trains; however, this is true only on average. The number of active pre-synaptic neurons is a random variable binomially distributed with average $n_A K$ and variance $n_A (1 - n_A) K$. Future developments of the theoretical approach reported here should include also such variability in modeling network dynamics [9].

Furthermore, we show that the considered model is not chaotic for instantaneous synapses; in such a case, we observe irregular asynchronous states due to stable chaos [63]. The system can become truly chaotic for only finite synaptic times [3, 30]. However, we report clear indications that for synapses faster than the membrane time constant τ_m the passage from mean-driven to fluctuation-driven dynamics is not related to the onset of chaos. Only for extremely slow synapses do we have numerical evidence that the appearance of the bursting regime could be related to a passage from a zero Lyapunov exponent to a positive one. This is in agreement with the results reported in [26, 31] for homogeneous inhibitory networks. These preliminary indications demand more detailed investigations of deterministic spiking networks in order to relate fluctuation-driven regimes and chaos onsets. Moreover, we expect that it will be hard to distinguish whether the erratic current fluctuations are due to regular chaos or stable chaos on the basis of network activity analysis, as also pointed out in [30].

Concerning the biological relevance of the presented model, we can attempt a comparison with experimental data obtained for MSNs in the striatum. This population of neurons is fully inhibitory with sparse lateral connections (connection probability $\simeq 10\%$–20% [77, 81]) that are unidirectional and relatively weak [78]. Furthermore, for MSNs within the same collateral network the axonal propagation delays are quite small $\simeq 1$–2 ms [76] and can be safely neglected. The dynamics of these neurons in behaving mice reveals a low average firing rate with irregular firing activity (bursting) with an associated large coefficient of variation [47]. As we have shown, these features can be reproduced by sparse networks of LIF neurons with sufficiently slow synapses at $g > g_m$ and $\tau_\alpha > \tau_m$. For values of the membrane time constant that are comparable to those measured for MSNs [59, 61] (namely, $\tau_m \simeq 10$–20 msec), the model is able to capture some of the main aspects of MSNs dynamics, as shown in table 1. We obtain a reasonable agreement with the experiments for sufficiently slow synapses, where the interaction among MSNs is mainly mediated by GABA$_A$ receptors, which are characterized by IPSP durations of the order of $\simeq 5$–20 ms [34, 81]. However, apart the burst duration, which is definitely shorter, all other aspects of the MSN dynamics can be already captured for $\tau_\alpha = 2\tau_m$ (with $\tau_m = 10$ ms), as shown in table 1. Therefore, we can safely affirm, as also suggested in [66], that the fluctuation-driven regime emerging at $g > g_m$ is the most appropriate in order to reproduce the dynamical evolution of this population of neurons.

Other inhibitory populations are present in the basal ganglia. In particular, two coexisting inhibitory populations, *arkypallidal* (Arkys) and *prototypical* (Protos) neurons, have been recently discovered in the external globus pallidus [43]. These populations have distinct physiological and dynamical characteristics, and have been shown to be fundamental for action suppression during the performance of behavioral tasks in rodents [44]. Protos are characterized by a high firing rate $\simeq 47$ Hz and a not too large coefficient of variation (namely, $CV \simeq 0.58$) both in awake and slow wave sleep (SWS) states; meanwhile, Arkys have clear bursting dynamics with $CV \simeq 1.9$ [18, 44]. Furthermore, the firing rate of Arkys is definitely larger in the awake state (namely, $\simeq 9$ Hz) with respect to the SWS state, where firing rates are $\simeq 3$–5 Hz [44].

On the basis of our results, on the one hand, Protos can be modeled as LIF neurons with reasonably fast synapses in a mean-driven regime, namely with synaptic coupling $g < g_m$. On the other hand, Arkys should be characterized by IPSP with definitely longer durations, and should be in a fluctuation-driven phase as suggested from the results reported in figure 11. Since, as shown in figure 11(a), the firing rate of inhibitory neurons decreases by increasing synaptic strength g, we expect that the passage from awake to SWS should be characterized by a reinforcement of Arkys synapses. Our conjectures about Arkys and Protos synaptic properties based on their dynamical behaviors ask for experimental verification, which we hope will happen shortly.

Besides the straightforward applicability of our findings to networks of pulse-coupled oscillators [48], it has been recently shown that LIF networks with instantaneous and non-instantaneous synapses can be transformed into the Kuramoto–Daido model [17, 35, 62]. Therefore, we expect that our findings should extend to phase oscillator arrays with repulsive coupling [79]. This will allow for a wider applicability of our results, due to the relevance of limit-cycle oscillators not only for modeling biological systems [86], but also for many scientific and technological applications [19, 58, 71, 74].

Acknowledgments

Appendix A. Event driven maps

By following [53, 91] the ordinary differential equations (1) and (2) describing the evolution of the membrane potential of neurons can be rewritten exactly as discrete time maps connecting successive firing events occurring in the network. In the following we will explicitly report such event driven maps for the case of instantaneous and α-synapses.

For instantaneous PSPs, the event driven map for neuron i takes the following expression:

$$v_i(n+1) = v_i(n)\mathrm{e}^{-T_\delta} + I_i(1 - \mathrm{e}^{-T_\delta}) - \frac{g}{K}C_{\mathrm{m}i}, \tag{16}$$

where the sequence of firing times $\{t_n\}$ in the network is denoted by the integer indices $\{n\}$, m is the index of the neuron firing at time t_{n+1}, and $T_\delta \equiv t_{n+1} - t_n$ is the ISI associated with two successive neuronal firings. This latter quantity is calculated from the following expression:

$$T_\delta = \ln\left[\frac{I_m - v_m}{I_m - 1}\right]. \tag{17}$$

For α-pulses, the evolution of the synaptic current $E_i(t)$, stimulating the i-th neuron can be expressed in terms of a second-order differential equation, namely

$$\ddot{E}_i(t) + 2\alpha\dot{E}_i(t) + \alpha^2 E_i(t) = \frac{\alpha^2}{K}\sum_{j\neq i}\sum_{n|t_n<t} C_{ij}\delta(t - t_n). \tag{18}$$

Equation (18) can be rewritten as two first-order differential equations by introducing the auxiliary variable $Q \equiv \dot{E}_i - \alpha E_i$, namely

$$\dot{E}_i = Q_i - \alpha E_i, \quad \dot{Q}_i = -\alpha Q_i + \frac{\alpha^2}{K}\sum_{n|t_n<t} C_{ij}\delta(t - t_n) \tag{19}$$

Finally, equations (1) and (19) can be exactly integrated from the time t_n, just after delivery of the n-th pulse, to time t_{n+1} corresponding to the emission of the $(n+1)$-th spike, to obtain the following event driven map:

$$Q_i(n+1) = Q_i(n)\mathrm{e}^{-\alpha T_\alpha} + \frac{\alpha^2}{K}C_{mi}, \tag{20a}$$

$$E_i(n+1) = E_i(n)\mathrm{e}^{-\alpha T_\alpha} + Q_i(n)T_\alpha\mathrm{e}^{-\alpha T_\alpha}, \tag{20b}$$

$$v_i(n+1) = v_i(n)\mathrm{e}^{-T_\alpha} + I_i(1 - \mathrm{e}^{-T_\alpha}) - gH_i(n). \tag{20c}$$

In this case, the ISI $T_\alpha \equiv t_{n+1} - t_n$ should be estimated by solving the following expression:

$$T_\alpha = \ln\left[\frac{I_m - v_m(n)}{I_m - gH_m(n) - 1}\right], \tag{21}$$

where the explicit expression for $H_i(n)$ appearing in equations (20c) and (21) is

$$H_i(n) = \frac{e^{-T_\alpha} - e^{-\alpha T_\alpha}}{\alpha - 1}\left(E_i(n) + \frac{Q_i(n)}{\alpha - 1}\right) - \frac{T_\alpha e^{-\alpha T_\alpha}}{\alpha - 1}Q_i(n). \tag{22}$$

The model so far introduced contains only adimensional units; however, the evolution equation for the membrane potential (1) can be easily re-expressed in terms of dimensional variables as follows:

$$\tau_m \dot{V}_i(\tilde{t}) = \tilde{I}_i - V_j(\tilde{t}) - \tau_m \tilde{g} \tilde{E}_i(\tilde{t}) \quad i = 1, \cdots, N, \tag{23}$$

where we have chosen $\tau_m = 10$ ms as the membrane time constant, and $\tilde{I}_i$ represents the neural excitability and external stimulation. Furthermore, $\tilde{t} = t \cdot \tau_m$, and the field $\tilde{E}_i = E_i/\tau_m$ has the dimensionality of a frequency and $\tilde{g}$ of a voltage. The currents $\{\tilde{I}_i\}$ also have the dimensionality of a voltage since they include the membrane resistance.

For the other parameters/variables the transformation to physical units is simply given by

$$V_i = V_r + (V_{th} - V_r)v_i, \tag{24}$$

$$\tilde{I}_i = V_r + (V_{th} - V_r)I_i, \tag{25}$$

$$\tilde{g} = (V_{th} - V_r)g, \tag{26}$$

where $V_r = -60$ mV and $V_{th} = -50$ mV are realistic values of the membrane reset and threshold potential. The isolated i-th LIF neuron is supra-threshold whenever $\tilde{I}_i > V_{th}$.

Appendix B. Average firing rate for instantaneous synapses

In this appendix, by following the approach in [70] we derive the average firing rate of a supra-threshold LIF neuron subject to inhibitory synaptic shot noise of constant amplitude G, namely

$$\dot{v}(t) = I - v(t) - G\sum_{\{t_k\}}\delta(t - t_k), \tag{27}$$

where $I > 1$. The post-synaptic pulses reaching the neuron are instantaneous and their arrival times are Poisson-distributed and characterized by a rate R. In order to find the firing rate response of the LIF neuron we introduce the probability density $P(v)$ and the flux $J(v)$ associated with the membrane potentials. These satisfy the following continuity equation:

$$\frac{\partial P}{\partial t} + \frac{\partial J}{\partial v} = \rho(t)[\delta(v - v_r) - \delta(v - \theta)], \tag{28}$$

where $\rho(t)$ is the instantaneous firing rate of the neuron. The flux can be decomposed in an average drift term plus the inhibitory part, namely

$$J = (I - v)P + J_{inh}, \tag{29}$$

$$\frac{\partial J_{inh}(v, t)}{\partial v} = R[P(v, t) - P(v - G, t)]. \tag{30}$$

The set of equations (28) to (30) is complemented by the boundary conditions

$$J(\theta, t) = \rho(t) \qquad J_{inh}(\theta, t) = 0 \qquad P(\theta, t) = 0,$$

and by the requirement that the membrane potential distribution should be normalized, i.e
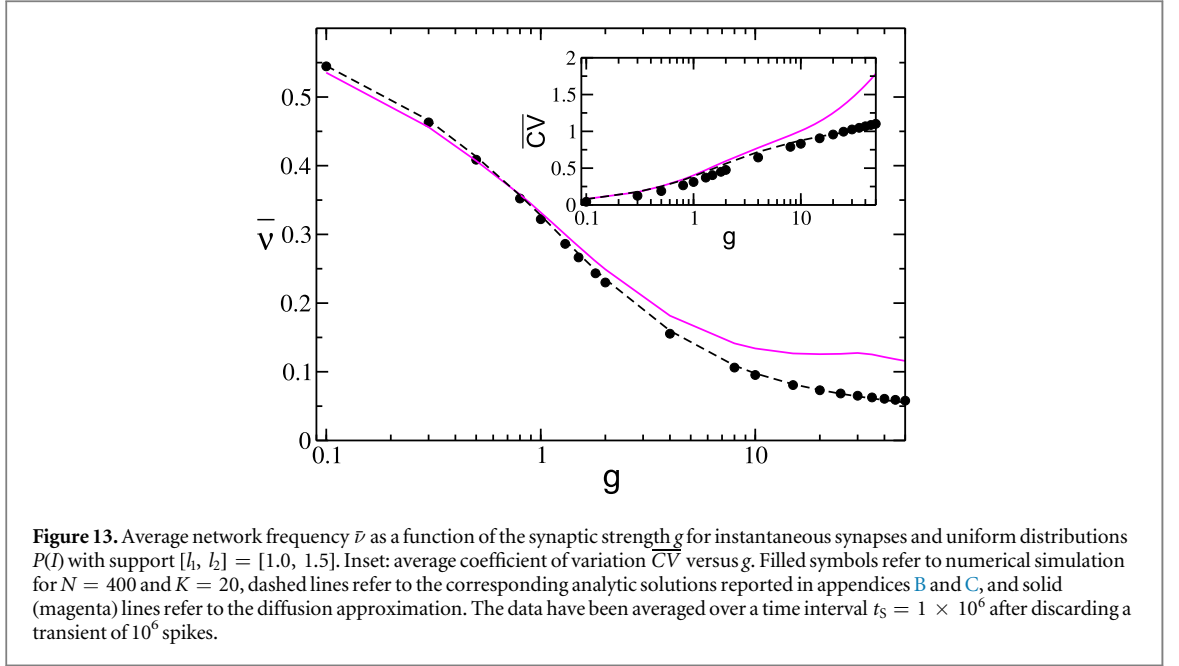
$$\int_{-\infty}^{\theta} P(v, t)dv = 1.$$

By introducing bilateral Laplace transforms $\tilde{f}(s) = \int_{-\infty}^{\infty} dv e^{sv} f(v)$ and by performing some algebra along the lines described in [70] it is possible to derive the analytic expression for the average firing rate

$$\frac{1}{\nu_0} = \int_0^\infty \frac{ds}{s}\frac{e^{s\theta} - e^{sv_r}}{\tilde{Z}_0(s)}, \tag{31}$$

where $\tilde{Z}_0(s)$ is the Laplace transform of the sub-threshold probability density. Namely, it reads as

$$\tilde{Z}_0(s) = C_0[s^{-R}e^{sI + R\mathcal{E}(Gs)}], \tag{32}$$

where $\mathcal{E}(y) = -\int_{-y}^{\infty} dt e^{-t}/t$ is the exponential integral, $C_0 = e^{-R(\Gamma + \ln G)}$ is the normalization constant ensuring that the distribution $Z_0(v)$ is properly normalized, and Γ is the Euler–Mascheroni constant.

Figure 13. Average network frequency $\bar{\nu}$ as a function of the synaptic strength g for instantaneous synapses and uniform distributions $P(I)$ with support $[l_1, l_2] = [1.0, 1.5]$. Inset: average coefficient of variation $\overline{CV}$ versus g. Filled symbols refer to numerical simulation for $N = 400$ and $K = 20$, dashed lines refer to the corresponding analytic solutions reported in appendices B and C, and solid (magenta) lines refer to the diffusion approximation. The data have been averaged over a time interval $t_S = 1 \times 10^6$ after discarding a transient of 10^6 spikes.

To validate this method and obtain the average firing frequency $\bar{\nu}$, we compare the theoretical estimates given by (14) with numerical data obtained for sparse networks with in-degree K and instantaneous inhibitory synapses. The agreement is quite remarkable, as shown in figure 13. In the same figure, the solid magenta line refers to the results obtained by employing the diffusion approximation [8, 9, 69, 80]: clear discrepancies are already evident for $g \geqslant 1$. In particular, for the diffusion approximation and the evaluation of (14) we assume that each neuron receives a Poissonian spike train with an arrival rate given by $R = n_A \bar{\nu} K$. Furthermore, it should be stressed that in this case we test the quality of the approach described in this appendix versus the diffusion approximation; therefore, n_A, required to estimate $\bar{\nu}$, is obtained from the simulation and not derived self-consistently as done in section 4.

Appendix C. Coefficient of variation for instantaneous synapses

In order to derive the coefficient of variation for the shot noise case it is necessary to obtain the first two moments of the first-passage-time density $q(t)$. By following the same approach as in appendix B, the time-dependent continuity equation with initial condition $P(v, 0) = v_r$ is written as

$$\frac{\partial P}{\partial t} + \frac{\partial J}{\partial v} = \rho(t)[\delta(v - v_r) - \delta(v - \theta)] + \delta(t)\delta(v - v_r). \tag{33}$$

As suggested in [70], equation (33) can be solved by performing a Fourier transform in time and a bilateral Laplace transform in membrane potential. This allows us to obtain the Fourier transform of the spike-triggered rate, namely

$$\hat{\rho}(\omega) = \frac{\int_0^\infty ds \, s^{i\omega} A'(s)}{\int_0^\infty ds \, s^{i\omega}[B'(s) - A'(s)]}, \tag{34}$$

where $A(s) = e^{s v_r}/\tilde{Z}_0(s)$ and $B(s) = e^{s\theta}/\tilde{Z}_0(s)$. The Fourier transform of the first-passage-time density is $\hat{q}(\omega) = \frac{\hat{\rho}(\omega)}{1 + \hat{\rho}(\omega)}$, and the first and second moment of the distribution are given by

$$\frac{\partial \hat{q}}{\partial \omega}\big|_{\omega=0} = -i\langle t \rangle, \tag{35}$$

$$\frac{\partial^2 \hat{q}}{\partial \omega^2}\big|_{\omega=0} = -\langle t^2 \rangle. \tag{36}$$

Since the integrals appearing in equation (34) cannot be exactly solved, we have expanded it to the second-order, obtaining

$$\hat{\rho}(\omega) \simeq \frac{n_0 + n_1\omega + n_2\omega^2}{d_0 + d_1\omega + d_2\omega^2}, \tag{37}$$

where $n_0 = -1$, $d_0 = 0$, $d_1 = -\mathrm{i}n_0/\nu_0$, and

$$n_1 = \mathrm{i} \int_0^\infty \log s A'(s)\,\mathrm{d}s, \tag{38}$$

$$d_2 = \int_0^\infty \frac{\log s}{s}[B(s) - A(s)]\,\mathrm{d}s. \tag{39}$$

From expression (34) we can finally obtain the first and second moment of $q(t)$, namely

$$\langle t \rangle = \frac{1}{\nu_0}, \quad \langle t^2 \rangle = 2[d_1^2 + d_2 + d_1 n_1]. \tag{40}$$

Once these quantities are known, the coefficient of variation can be easily estimated for each neuron with excitability I.

The results obtained for the average coefficient of variation $\overline{CV}$ for a sparse network are compared with numerical data and with the diffusion approximation in the inset of figure 13. It is evident that the approximation derived here is definitely more accurate than the diffusion approximation for synaptic strengths larger than $g \simeq 1$.

Appendix D. Average firing rate for slow synapses

In section 5 we have examined the average activity of the network for non-instantaneous IPSPs with α-function profiles. In the presence of synaptic filtering, whenever the synaptic time constant is larger than the membrane time constant, one can apply the so-called adiabatic approach to derive the firing rate ν_0 of a single neuron, as described in [50, 51].

In this approximation, the output firing rate ν_0 of the single neuron driven by a slowly varying stochastic input current z with an arbitrary distribution $P(z)$ is given by

$$\nu_0 \simeq \int \mathrm{d}z P(z)\nu(z), \tag{41}$$

where $\nu(z)$ is the input to rate transfer function of the neuron under a stationary input which for the LIF neuron is simply

$$\nu(z) = \left[\ln\left(\frac{z - \nu_\mathrm{r}}{z - \theta}\right)\right]^{-1}. \tag{42}$$

The synaptic filtering induces temporal correlations in the input current z, which can be written as

$$\langle (z(t) - \mu)(z(t') - \mu) \rangle = \frac{\sigma^2}{2\tau_\mathrm{s}}\exp\left[-\frac{|t - t'|}{\tau_\mathrm{s}}\right]. \tag{43}$$

Here τ_s is the synaptic correlation time. In the case of α-pulses, where the rise and decay synaptic times coincide, we can assume that the correlation time is given by $\tau_\mathrm{s} = \tau_\mathrm{P} = 2\tau_\alpha$.

Analogous to the diffusion approximation [8, 9, 14], the input currents are approximated as a Gaussian noise with mean μ and variance $\sigma_z^2 = \sigma/2\tau_\mathrm{s}$. In our network model, a single neuron receives an average current μ given by equation (4) with a standard deviation σ given by equation (10). In particular, the fraction of active neurons n_A entering in the expressions of μ and σ is in this case obtained by numerical simulations.

Therefore, the single neuron output firing rate reads as

$$\nu_0(I) = \int \frac{\mathrm{d}z}{\sqrt{2\pi}\,\sigma_z}\mathrm{e}^{-\frac{(z - \mu(I))^2}{2\sigma_z^2}}\left[\ln\left(\frac{z - \nu_\mathrm{r}}{z - \theta}\right)\right]^{-1}, \tag{44}$$

where I is the neuronal excitability.

The average firing rate of the LIF neurons in the network, characterized by an excitability distribution $P(I)$, can be estimated as

$$\bar{\nu} = \int_{\{I_\mathrm{A}\}} \mathrm{d}I\, P(I) \int_\theta \frac{\mathrm{d}z}{\sqrt{2\pi}\,\sigma_z}\mathrm{e}^{-\frac{(z - \mu(I))^2}{2\sigma_z^2}}\left[\ln\left(\frac{z - \nu_\mathrm{r}}{z - \theta}\right)\right]^{-1}, \tag{45}$$

where we impose the self-consistent condition that the average output frequency is equal to that of the average input.

References

[1] Angulo-Garcia D, Berke J D and Torcini A 2015 Cell assembly dynamics of sparsely-connected inhibitory networks: a simple model for the collective activity of striatal projection neurons *PLoS Comput. Biol.* **12** e1004778

[2] Angulo-Garcia D and Torcini A 2015 Stochastic mean-field formulation of the dynamics of diluted neural networks *Phys. Rev. E* **91** 022928

[3] Angulo-Garcia D and Torcini A 2014 Stable chaos in fluctuation driven neural circuits *Chaos, Solitons Fractals* **69** 233–45

[4] Benettin G, Galgani L, Giorgilli A and Strelcyn J-M 1980 Lyapunov characteristic exponents for smooth dynamical systems and for hamiltonian systems; a method for computing all of them. Part 1: theory *Meccanica* **15** 9–20

[5] Berke J D, Okatan M, Skurski J and Eichenbaum H B 2004 Oscillatory entrainment of striatal neurons in freely moving rats *Neuron* **43** 883–96

[6] Bressloff P C and Coombes S 2000 Dynamics of strongly coupled spiking neurons *Neural Comput.* **12** 91–129

[7] Bressloff P C and Coombes S 2000 A dynamical theory of spike train transitions in networks of integrate-and-fire oscillators *SIAM J. Appl. Math.* **60** 820–41

[8] Brunel N 2000 Dynamics of sparsely connected networks of excitatory and inhibitory spiking neurons *J. Comput. Neurosci.* **8** 183–208

[9] Brunel N and Hakim V 1999 Fast global oscillations in networks of integrate-and-fire neurons with low firing rates *Neural. Comput.* **11** 1621–71

[10] Bullmore E and Sporns O 2009 Complex brain networks: graph theoretical analysis of structural and functional systems *Nat. Rev. Neurosci.* **10** 186–98

[11] Burkitt A N 2006 A review of the integrate-and-fire neuron model: I. Homogeneous synaptic input *Biol. Cybern.* **95** 1–19

[12] Buzsáki G and Draguhn A 2004 Neuronal oscillations in cortical networks *Science* **304** 1926–9

[13] Camazine S 2003 *Self-Organization in Biological Systems* (Princeton, NJ: Princeton University Press)

[14] Capocelli R M and Ricciardi L M 1971 Diffusion approximation and first passage time problem for a model neuron *Kybernetik* **8** 214–23

[15] Carrillo-Reid L, Tecuapetla F, Tapia D, Hernández-Cruz A, Galarraga E, Drucker-Colin R and Bargas J 2008 Encoding network states by striatal cell assemblies *J. Neurophysiol.* **99** 1435–50

[16] Coultrip R, Granger R and Lynch G 1992 A cortical model of winner-take-all competition via lateral inhibition *Neural Netw.* **5** 47–54

[17] Daido H 1996 Onset of cooperative entrainment in limit-cycle oscillators with uniform all-to-all interactions: bifurcation of the order function *Physica D* **91** 24–66

[18] Dodson P D, Larvin J T, Duffell J M, Garas F N, Doig N M, Kessaris N, Duguid I C, Bogacz R, Butt S J B and Magill P J 2015 Distinct developmental origins manifest in the specialized encoding of movement by adult neurons of the external globus pallidus *Neuron* **86** 501–13

[19] Dörfler F and Bullo F 2014 Synchronization in complex networks of phase oscillators: a survey *Automatica* **50** 1539–64

[20] Ermentrout B 1992 Complex dynamics in winner-take-all neural nets with slow inhibition *Neural Netw.* **5** 415–31

[21] Fukai T and Tanaka S 1997 A simple neural network exhibiting selective activation of neuronal ensembles: from winner-take-all to winners-share-all *Neural Comput.* **9** 77–97

[22] Golomb D, Hansel D and Mato G 2001 Mechanisms of synchrony of neural activity in large networks *Handb. Biol. Phys.* **4** 887–968

[23] Golomb D and Rinzel J 1994 Clustering in globally coupled inhibitory neurons *Physica D* **72** 259–82

[24] Grzywacz N M and Yuille A L 1990 A model for the estimate of local image velocity by cells in the visual cortex *Proc. R. Soc. London, Ser. B* **239** 129–61

[25] Hänggi P, Talkner P and Borkovec M 1990 Reaction-rate theory: fifty years after Kramers *Rev. Mod. Phys.* **62** 251

[26] Harish O and Hansel D 2015 Asynchronous rate chaos in spiking neuronal circuits *PLoS Comput. Biol.* **11** e1004266

[27] Harris-Warrick R M 1992 *Dynamic Biological Networks: The Stomatogastric Nervous System* (Cambridge, MA: MIT Press)

[28] Itti L and Koch C 2001 Computational modelling of visual attention *Nat. Rev. Neurosci.* **2** 194–203

[29] Jahnke S, Memmesheimer R-M and Timme M 2008 Stable irregular dynamics in complex neural networks *Phys. Rev. Lett.* **100** 048102

[30] Jahnke S, Memmesheimer R-M and Timme M 2009 How chaotic is the balanced state? *Front. Comp. Neurosci.* **3**

[31] Kadmon J and Sompolinsky H 2015 Transition to chaos in random neuronal networks *Phys. Rev. X* **5** 041030

[32] Kerner B S and Osipov V V 1990 Self-organization in active distributed media: scenarios for the spontaneous formation and evolution of dissipative structures *Phys.-Usp.* **33** 679–719

[33] Komarov M A, Osipov G V and Suykens J A K 2009 Sequentially activated groups in neural networks *EPL* **86** 60006

[34] Koos T, Tepper J M and Wilson C J 2004 Comparison of ipscs evoked by spiny and fast-spiking neurons in the neostriatum *J. Neurosci.* **24** 7916–22

[35] Kuramoto Y 1984 *Chemical Oscillations, Waves, and Turbulence* vol 19 (New York: Springer Science & Business Media)

[36] Lanciego J L, Luquin N and Obeso J A 2012 Functional neuroanatomy of the basal ganglia *Cold Spring Harbor Perspect. Med.* **2** a009621

[37] Larremore D B, Shew W L, Ott E, Sorrentino F and Restrepo J G 2014 Inhibition causes ceaseless dynamics in networks of excitable nodes *Phys. Rev. Lett.* **112** 138103

[38] Laughlin S B and Sejnowski T J 2003 Communication in neuronal networks *Science* **301** 1870–4

[39] Laurent G 2002 Olfactory network dynamics and the coding of multidimensional signals *Nat. Rev. Neurosci.* **3** 884–95

[40] Lindner B 2006 Superposition of many independent spike trains is generally not a Poisson process *Phys. Rev. E* **73** 022901

[41] Luccioli S, Olmi S, Politi A and Torcini A 2012 Collective dynamics in sparse networks *Phys. Rev. Lett.* **109** 138103

[42] Luccioli S and Politi A 2010 Irregular collective behavior of heterogeneous neural networks *Phys. Rev. Lett.* **105** 158104

[43] Mallet N, Micklem B R, Henny P, Brown M T, Williams C, Bolam J P, Nakamura K C and Magill P J 2012 Dichotomous organization of the external globus pallidus *Neuron* **74** 1075–86

[44] Mallet N, Schmidt R, Leventhal D, Chen F, Amer N, Boraud T and Berke J D 2016 Arkypallidal cells send a stop signal to striatum *Neuron* **89** 308–16

[45] Marder E and Bucher D 2001 Central pattern generators and the control of rhythmic movements *Curr. Biol.* **11** R986–96

[46] Meinhardt H 1982 *Models of Biological Pattern Formation* vol 6 (London: Academic)

[47] Miller B R, Walker A G, Shah A S, Barton S J and Rebec G V 2008 Dysregulated information processing by medium spiny neurons in striatum of freely behaving mouse models of Huntington's disease *J. Neurophysiol.* **100** 2205–16

[48] Mirollo R E and Strogatz S H 1990 Synchronization of pulse-coupled biological oscillators *SIAM J. Appl. Math.* **50** 1645–62

[49] Monteforte M and Wolf F 2012 Dynamic flux tubes form reservoirs of stability in neuronal circuits *Phys. Rev. X* **2** 041007

[50] Moreno-Bote R and Parga N 2004 Role of synaptic filtering on the firing response of simple model neurons *Phys. Rev. Lett.* **92** 028102

[51] Moreno-Bote R and Parga N 2010 Response of integrate-and-fire neurons to noisy inputs filtered by synapses with arbitrary timescales: firing rate and correlations *Neural Comput.* **22** 1528–72

[52] Nowotny T and Rabinovich M I 2007 Dynamical origin of independent spiking and bursting activity in neural microcircuits *Phys. Rev. Lett.* **98** 128106

[53] Olmi S, Politi A and Torcini A 2014 Linear stability in networks of pulse-coupled neurons *Front. Comput. Neurosci.* **8** 8

[54] Olmi S, Angulo-Garcia D, Imparato A and Torcini A 2017 Exact firing time statistics of neurons driven by discrete inhibitory noise *Scientific Reports* in press (https://doi.org/10.1101/116467)

[55] Olmi S, Livi R, Politi A and Torcini A 2010 Collective oscillations in disordered neural networks *Phys. Rev.* E **81** 046119

[56] Ostojic S 2014 Two types of asynchronous activity in networks of excitatory and inhibitory spiking neurons *Nat. Neurosci.* **17** 594–600

[57] Parent A and Hazrati L-N 1995 Functional anatomy of the basal ganglia: l. The cortico-basal ganglia-thalamo-cortical loop *Brain Res. Rev.* **20** 91–127

[58] Pikovsky A and Rosenblum M 2015 Dynamics of globally coupled oscillators: progress and perspectives. Chaos: an Interdisciplinary *J. Nonlinear Sci.* **25** 097616

[59] Planert H, Berger T K and Silberberg G 2013 Membrane properties of striatal direct and indirect pathway neurons in mouse and rat slices and their modulation by dopamine *PloS One* **8** e57054

[60] Plenz D 2003 When inhibition goes incognito: feedback interaction between spiny projection neurons in striatal function *Trends Neurosci.* **26** 436–43

[61] Plenz D and Kitai S T 1998 Up and down states in striatal medium spiny neurons simultaneously recorded with spontaneous activity in fast-spiking interneurons studied in cortex-striatum-substantia nigra organotypic cultures *J. Neurosci.* **18** 266–83

[62] Politi A and Rosenblum M 2015 Equivalence of phase-oscillator and integrate-and-fire models *Phys. Rev.* E **91** 042916

[63] Politi A and Torcini A 2010 Stable chaos *Nonlinear Dynamics and Chaos: Advances and Perspectives* (New York: Springer) p 103–29

[64] Ponzi A and Wickens J 2010 Sequentially switching cell assemblies in random inhibitory networks of spiking neurons in the striatum *Journal Neurosci.* **30** 5894–911

[65] Ponzi A and Wickens J 2012 Input dependent cell assembly dynamics in a model of the striatal medium spiny neuron network *Front. Syst. Neurosci.* **6**

[66] Ponzi A and Wickens J R 2013 Optimal balance of the striatal medium spiny neuron network *PLoS Comput. Biol.* **9** e1002954

[67] Rabinovich M I and Varona P 2011 Robust transient dynamics and brain functions *Front. Comput. Neurosci.* **5** 24

[68] Renart A, Moreno-Bote R, Wang X-J and Parga N 2007 Mean-driven and fluctuation-driven persistent activity in recurrent networks *Neural. Comput.* **19** 1–46

[69] Ricciardi L M 2013 *Diffusion Processes and Related Topics in Biology* vol 14 (Berlin: Springer)

[70] Richardson M J E and Swarbrick R 2010 Firing-rate response of a neuron receiving excitatory and inhibitory synaptic shot noise *Phys. Rev. Lett.* **105** 178102

[71] Rodrigues F A, Peron T K D M, Ji P and Kurths J 2016 The Kuramoto model in complex networks *Phys. Rep.* **610** 1–98

[72] Shu Y, Hasenstaub A and McCormick D A 2003 Turning on and off recurrent balanced cortical activity *Nature* **423** 288–93

[73] Somogyi P, Tamas G, Lujan R and Buhl E H 1998 Salient features of synaptic organisation in the cerebral cortex *Brain Res. Rev.* **26** 113–35

[74] Strogatz S H 2001 Exploring complex networks *Nature* **410** 268–76

[75] Tattini L, Olmi S and Torcini A 2012 Coherent periodic activity in excitatory Erdos–Renyi neural networks: the role of network connectivity *Chaos* **22** 023133

[76] Taverna S, Ilijic E and Surmeier D J 2008 Recurrent collateral connections of striatal medium spiny neurons are disrupted in models of Parkinson's disease *J. Neurosci.* **28** 5504–12

[77] Taverna S, Van Dongen Y C, Groenewegen H J and Pennartz C M A 2004 Direct physiological evidence for synaptic connectivity between medium-sized spiny neurons in rat nucleus accumbens *in situ J. Neurophysiol.* **91** 1111–21

[78] Tepper J M, Koós T and Wilson C J 2004 Gabaergic microcircuits in the neostriatum *Trends Neurosci.* **27** 662–9

[79] Tsimring L S, Rulkov N F, Larsen M L and Gabbay M 2005 Repulsive synchronization in an array of phase oscillators *Phys. Rev. Lett.* **95** 014101

[80] Tuckwell H C 2005 *Introduction to Theoretical Neurobiology: Volume 2, Nonlinear and Stochastic Theories* vol 8 (Cambridge: Cambridge University Press)

[81] Tunstall M J, Oorschot D E, Kean A and Wickens J R 2002 Inhibitory interactions between spiny projection neurons in the rat striatum *J. Neurophysiol.* **88** 1263–9

[82] Ullner E and Politi A 2016 Self-sustained irregular activity in an ensemble of neural oscillators *Phys. Rev.* X **6** 011015

[83] van Vreeswijk C 1996 Partial synchronization in populations of pulse-coupled oscillators *Phys. Rev.* E **54** 5522–37

[84] Vanag V K, Yang L, Dolnik M, Zhabotinsky A M and Epstein I R 2000 Oscillatory cluster patterns in a homogeneous chemical system with global feedback *Nature* **406** 389–91

[85] Wang X-J and Buzsáki G 1996 Gamma oscillation by synaptic inhibition in a hippocampal interneuronal network model *J. Neurosci.* **16** 6402–13

[86] Winfree A T 2001 *The Geometry of Biological Time* vol 12 (New York: Springer Science & Business Media)

[87] Xiong Y, Huang C-H, Iglesias P A and Devreotes P N 2010 Cells navigate with a local-excitation, global-inhibition-biased excitable network *Proc. Natl Acad. Sci.* **107** 17079–86

[88] Yuille A L and Grzywacz N M 1989 A winner-take-all mechanism based on presynaptic inhibition feedback *Neural Comput.* **1** 334–47

[89] Zillmer R, Brunel N and Hansel D 2009 Very long transients, irregular firing, and chaotic dynamics in networks of randomly connected inhibitory integrate-and-fire neurons *Phys. Rev.* E **79** 031909

[90] Zillmer R, Livi R, Politi A and Torcini A 2006 Desynchronization in diluted neural networks *Phys. Rev.* E **74** 036203

[91] Zillmer R, Livi R, Politi A and Torcini A 2007 Stability of the splay state in pulse-coupled networks *Phys. Rev.* E **76** 046102